UNIVERSITÀ della CALABRIA
Facoltà di Ingegneria
Dipartimento di Meccanica

Scuola di Dottorato "Pitagora" in Scienze Ingegneristiche

Dottorato di Ricerca in Ingegneria Meccanica XXI Ciclo

SETTORE SCIENTIFICO DISCIPLINARE: ING-IND/16

Tesi di Dottorato

Fundamental Aspects in Metal Cutting Modelling

Coordinatore
Prof. Sergio Rizzuti

Supervisore
Prof. Luigino Filice

Candidata
Ing. Stefania Rizzuti

Dissertazione finale sottomessa per ottenere il titolo di Dottore di Ricerca in Ingegneria Meccanica
Anno Accademico 2007/2008

CONTENTS

INTRODUCTION

Machining is one of the most common manufacturing processes. Nearly every mechanical component in use has undergone a machining operation at some stage of its manufacturing process. Therefore, the effectiveness of metal cutting process significantly affects the overall cost of final products, and there is a strong drive to reduce time and cost of machining operations.

In the past century, a great deal of research has been devoted toward understanding the mechanics of metal cutting, with the objective of obtaining more effective cutting tools and more efficient manufacturing process plans. Traditionally, these objectives have been achieved by experimentation and prototyping. In spite of extensive research in this field, the basic mechanics of the cutting process and the interaction of many factors which leads to its great variety is not yet totally understood.

Understanding of cutting mechanics has caught the attention of many researchers, and many analytical, empirical and numerical models have been contributed to the knowledge in this field. While all these models have advanced the common knowledge about the cutting process, the suitability of a cutting model depends on prediction of machining performance in order to facilitate effective planning of machining operations achieving optimal productivity, quality and cost. In particular, numerical modelling of this process has attracted the attention of many researchers in recent years, because of the better insight it can provide into the mechanics of chip formation by avoiding many of the simplifications needed in other approaches. However, the reliability of a numerical cutting model is dependent on two factors; the reliability of the input data in terms

of material and frictional characteristics, and the correctness and efficiency of the numerical approach, formulation and procedures used.

This dissertation deals with some fundamental aspects of the numerical simulation of the cutting process, which constitute, up to now, a big challenge for the researchers involved in this field. The aim is to supply a useful scientific contribution to the ever-increasing need of reliable, robust and ready-to-use simulation tools. In particular, the achieved specific objectives of the proposed research are:

- analysis of the role played by the friction models within the numerical simulation of orthogonal cutting. The investigation deal with the prediction of both mechanical and thermal variables;
- development of a physically-consistent model for the global heat transfer coefficient, by means of an inverse approach based on a set of experimental data and on a mixed updated Lagrangian - Eulerian approach. The model was validated through its direct implementation in the FE code and its application in tool wear prediction;
- development of a numerical strategy for the identification of a simplified material law to properly define the behaviour of the workpiece material, utilizing only machining tests and taking also into account the thermal phenomena involved in the process.

This research has been performed at the Department of Mechanical Engineering of the University of Calabria and during research visit at the "Laboratoire de Mécanique des Systèmes et des Procédés (LMSP), at ENSAM (Ecole Nationale Supérieure d'Arts et Métiers), Paris, directed by Prof. F. Chinesta.

The results of the PhD activity were also possible thanks to the significant collaboration with other Italian research centres, namely the Department of Mechanical Technology, Production and Management Engineering, University of Palermo, the Department of Production Systems and Economics, Polytechnic of Torino and Institute of Science and Technology of Ceramics, CNR-Torino, and the Department of Mechanical Engineering, University of Brescia.

CHAPTER 1

FINITE ELEMENT SIMULATION OF METAL CUTTING

1.1 INTRODUCTION

It is recognized that machining operations play a leading role in manufacturing. A study carried out in 1998 by Merchant [1] showed that about 15% of the value of all the mechanical components manufactured worldwide is achieved through machining. Probably this quota increased in the last decade due to the increase of machining market and the demands of the manufacturing industries for micro and nano-machining [2]. As a consequence of its large economic and technical importance, a great number of researches have been carried out in order to optimize machining process in terms of improved quality, increased productivity and reduced cost [2].

A research conducted by Armarego et al. [3], in the USA in 1996, revealed the following important factors: the cutting tool was properly selected less than in 50% of the cases, the tool was used at the rated cutting speed only in the 58% of the cases, and finally only 38% of the tools were used up to their full tool-life capability. Since then many efforts have been done in this direction, but the situation still urges the need for developing more scientific approaches in order to improve machining performance.

Moreover, accurate predictions of the results of the machining operations are required. This approach relies strongly on the prediction of the accuracy of shape and dimensions, and the surface finish and properties of the subsurface layer of the parts produced, the machining times required and the costs of the operation performed. In general, existing methods for the control of manufacturing operations, mainly based on the experience and craftsmanship of the manufacturing engineers/machinists, are becoming obsolete and have to be replaced by science-/knowledge- based methods. These are the main reasons for the development and introduction of CAD/CAM/CAPP systems to support process planning and control in flexible manufacturing/machining systems capable of performing a large variety of machining operations [4].

It is expected that future production will unquestionably require rapid and reliable adaptation to technological innovations, and these will be essential for a continued existence in the marketplace. Consequently, much more effort must be made to consider available process knowledge in order to improve component properties, and process parameters have to be based on product-related production requirements [5]. One way of meeting these numerous requirements is to use modelling, with the following purposes [6]:

- To find ways of optimizing process quickly and realistically.
- To permit realistic predictions of process results.
- To obtain new knowledge of process steps and process design.
- To derive capabilities of process monitoring and control from this.

For the past 50 years metal cutting researchers have developed many modelling techniques including analytical techniques, slip-line solutions, empirical approaches, and finite element techniques.

In particular, several enhancements have been obtained in the last decade thank to the use of Finite Element simulation, which was used by numerous researchers to predict some typical machining variables, such as cutting forces, chip morphology, surface integrity, etc. [7].

1.2 MODELLING OF CUTTING PROCESSES

Metal cutting is a highly non-linear and coupled thermo-mechanical process, where the mechanical work is converted into heat through the plastic deformation involved during chip formation and also due to frictional work between the tool, chip and workpiece.

A thorough understanding of the material removal process in metal cutting is essential in selecting the tool material and in design, and also in assuring consistent dimensional accuracy and surface integrity of the finished product.

The earliest analytical models explaining the mechanical of metal cutting were proposed by Merchant [8,9], Piispanen [10], and Lee and Shaffer [11]. These models are known as shear angle models; they relate the chip shear angle to the tool rake angle. Kudo [12] introduced curved shearing to account for the controlled contact between the curved chip and the straight tool face. These models assumed rigid-perfectly plastic material behaviour.

Analytical models including the effect of work hardening and strain-rate effects were proposed by Palmer and Oxley [13] and Oxley et al. [14]. Interfacial friction along the toll-chip interface was incorporated into these viscoplastic models by Doyle et al. [15]. The effect of heating in metal cutting was included in an analytical model by Trigger and Chao [16]. Three-dimensional geometric conditions in metal cutting were considered by Usui et al. [17] using an energy approach.

In recent years, the finite element method has become the main tool for simulating metal cutting processes.

An important aspect of finite element simulation of metal cutting is the type of numerical formulation used, because of the great implications it has in the success of such analyses.

Typical approaches for numerical modelling of metal cutting process are Lagrangian and Eulerian techniques, as well as a combination of both called the

arbitrary Lagrangian-Eulerian formulation (denoted in the literature by the acronym ALE) [18,19].

In Lagrangian approach, the mesh follows the material, it is "attached to the workpiece". In the updated Lagrangian formulation, because the elements move with the workpiece, they experience both large plastic deformation and rigid body motion. Under such circumstances, the larger deformation, and the changing material properties due to stress and strain in the material, need to be considered. The advantage of the updated Lagrangian formulation is that the tool can be simulated from the start of the cutting to a steady state. [20] But in order to extend the cutting time until steady state, the model requires large computational times. In addition, in order to perform chip separation, material failure and separation criteria are necessary. An other problem in the Lagrangian formulation is the computational instability due to the large distortion of some elements. This problem may eventually cause unrealistic results or premature termination of the analysis. Severe element distortion also results in a degradation of the accuracy. To address this issue it is useful to redefine the mesh system periodically, and so algorithms of remeshing and rezoning have to be included in the finite element codes.

The first model for orthogonal cutting utilizing simulated chip formation from the incipient stage to the steady state was due to Strenkowski and Carroll [21]. In their study, no heat was assumed to be conducted between chip and workpiece. The values of the chip separation criterion based on effective plastic strain were used to simulate the cutting process, without comparison to experiments. When it exceeded a specified value at the nodes closest to the tool tip, the nodes would be separated to form the machined surface and chip underneath. They found that different values selected for chip separation criterion based on the effective plastic strain affect the magnitude of the residual stresses in the machined surface of the workpiece. Strenkowski and Mitchum [22] presented the modified cutting model. They analyzed the transition from indentation to incipient cutting and used their results to evaluate the values for the chip separation criterion. Their results

showed that the criterion value, based on the effective plastic strain, increases with depth of cut.

Lin and Lin [23] developed a thermo-elastic-plastic cutting model. The finite difference method was adopted to determine the temperature distribution within the chip and the tool. In their model, a chip separation criterion based on the strain energy density was introduced. They verified that the chip separation criterion value based on the strain energy density was a material constant and was independent of uncut chip thickness. With this cutting model, Lin and Pan [24,25] simulated an entire orthogonal cutting process with tool frank wear from incipient stage to the steady state. The agreement between simulation and experimental results for cutting forces, friction force, the chip thickness, and contact length was found to be acceptable. Lin and Liu [26] analyzed an orthogonal finish machining using tungsten carbide and diamond tools that had different coefficients of thermal conductivity. Comparing the cutting forces predicted by the model with those obtained by experiment for orthogonal finish machining, they showed that the model could simulate the orthogonal finish machining process for different tool materials.

Ueda and Manabe [27] simulated the oblique cutting process as the first step in the three dimensional deformation analysis of cutting. With a displacement-based criterion, the chip formation process is continuously simulated from the beginning of the cutting until the steady state. When the distance between the tool tip and the nodal point located immediately in front exceeded a predefined critical value of separation, the nearest element was separated. However, the physics of a displacement-based chip separation criterion has not been clearly characterized. The results of the rigid plastic finite element analysis are qualitatively compared with in situ scanning electron microscope observation of the cutting experiments.

Zhang and Bagchi [28] developed conditional link elements handling chip separation from the workpiece. A displacement-based chip separation criterion was used to selectively null the link elements as the tool progressed. The validity of this model was examined by comparing the calculated cutting force, feed force,

shear angle, and plastic deformation with those from experiments. But because this model ignored the temperature and strain rate effects, it was only useful for low-speed machining.

Hashemi et al. [29] presented the first cutting model that did not assume a predefined cutting path. A unique chip fracture algorithm was implemented to permit tool travel between any set of nodes and t allow segmentation of the chip. Although a number of important features such as friction, temperature effects, and workpiece strain hardening were neglected and an overly coarse mesh that restricted the number of potential tool pathways was used, this model was thought to be a considerable achievement.

In Eulerian approach, the mesh is fixed spatially and the material flows through the mesh. Eulerian approach is suitable to analyse the steady state of cutting process, not including the transition from initial to steady state cutting process. Cutting process analysis with Eulerian approach requires less calculation time because the workpiece model consists of fewer elements. That is the reason why before 1995 the applications of Eulerian approach in chip formation analysis overrun those of Lagrangian approach. But experimental work is often necessary in order to determine the chip geometry and shear angle, which is an unavoidable part of geometry modelling.

The first application of the approach to metal cutting using a viscoplastic material model was reported by Strenkowski and Carroll [30]. This model is the so-called Eulerian cutting model. As this approach considers each element to be a fixed control volume, such that the mesh does not move with the flowing material as with the Lagrangian approach, the boundaries of the chip must be known in advance. These researchers later investigated the correlation between the Lagrangian and Eulerian frames. Both approaches showed reasonably good correlation with experimental results for cutting forces, residual stresses and strains, and chip geometry. With the Eulerian approach, Strenkowski and Moon [31] analyzed steady-state orthogonal cutting with the capability to predict chip geometry and chip-tool contact length for purely viscoplastic materials.

In 1991, Komvopoulos and Erpenbeck [32] investigated steady-state cutting effects of cratered tools with built-up edges. They examined the effects of material constitutive behaviour for rate-independent elastic-perfectly-plastic materials and rate-sensitive elastic-plastic isotropically strain hardening material. The analysis assumed an initially stress-free steady-state chip geometry and modelled a relatively short progression of the tool. A displacement-based chip separation criterion was used, and good correlation with experimental results was achieved.

Moriwaki et al. [33], developed a rigid plastic finite-element model to simulate the orthogonal micro-cutting process and examined the effects of the tool edge radius to depth of cut in the micro cutting process. They also analyzed the flow of cutting heat and temperature distribution. In analyzing temperature, however, they did not consider the variation of the flow stress with temperatures and the velocities in workpiece and chip and, hence, their study was for very low cutting speeds.

Shih and Yang [34] developed a plane strain steady-state cutting model using a displacement-based chip separation criterion. Consideration of strain rate, temperature, and friction effects was combined with a clever remeshing scheme to allow efficient analysis of very long cutting lengths. To improve the accuracy of residual stresses, workpiece cooling was considered. Recently, a more realistic stick-slip friction model was incorporated, together with an unbalanced force reduction technique that stabilized the chip separation process [35]. Contour plots and an Eulerian description of the material deformation were also presented to gain better understanding of the metal cutting mechanics [36].

Joshi et al. [37] calculated the strain rates and stresses in the primary shear deformation zone and compared them with the known experimental results for orthogonal steady-state machining. The material behaviour in the metal cutting process was modelled by a viscoplastic constitutive equation.

Wu et al. [38] developed a thermo-viscoplastic model of the orthogonal machining process based on a three-field, mixed, finite element method. This

method was highly accurate for coarse meshes, computationally very cheap, and did not suffer from locking for incompressible materials. It also satisfied the nontrivial stress boundary condition better than the compatible displacement model. From this model, detailed information about the stress, strain rate, temperature, cutting forces, chip thickness, shear angle, contact length, chip geometry, and heat conduction could be obtained. Simulations were performed for aluminum 6061 alloy and pure titanium. Kim and Sin [39] developed a cutting model by applying the thermo-viscoplastic FEM to analyze the mechanics of the steady-state orthogonal cutting process. The model was capable of dealing with free chip geometry and chip-tool contact length. The coupling with thermal effects was also considered. In analyzing temperature distributions, the "upwind" scheme was employed and hence it was possible to analyze high-speed metal cutting. For 0.2% carbon steel, good correlation between experiments and simulations was found.

The arbitrary Lagrangian-Eulerian (ALE) approach is a general formulation that combines the features of pure Lagrangian and Eulerian approach. The nodal points of the FE mesh are neither attached to the material points nor are they fixed in space. The mesh is allowed to move independently of the material. The flexibility of ALE description in adaptation of the finite element mesh provides a powerful tool for performing many difficult analyses involving large deformation problems.

1.3 CRITICAL ASPECTS OF THE NUMERICAL SIMULATION

Simulation of forming operations has reached high accuracy and robustness being able to consider contact interfaces, non isothermal and strain rate dependent processes, complex component geometries (3D models are nowadays efficient and reliable as 2D codes) and damage modelling. The use of Finite Element Method (FEM) codes for simulating plastic deformation processes helps in the identification of best die geometries and process parameters so reducing the trial and error refining as well as increasing the part quality.

In the last two decades, the Finite Element Method (FEM) has also been applied to simulate various cutting processes [21, 40, 41, 42]. It has been shown that the FEM cutting simulation can be used to estimate the process variables that are very difficult to measure during cutting, such as tool stresses and temperature, chip temperature, and chip sliding velocity along the tool face. The knowledge of these cutting variables provides an insightful understanding of the cutting mechanics and allows the analysis of tool wear. Furthermore, their correlations with tool wear/tool life can facilitate researchers to conduct a systematic process optimization [48].

Figure 1.1 depicts the relevant input properties/parameters required for a designed cutting simulation.

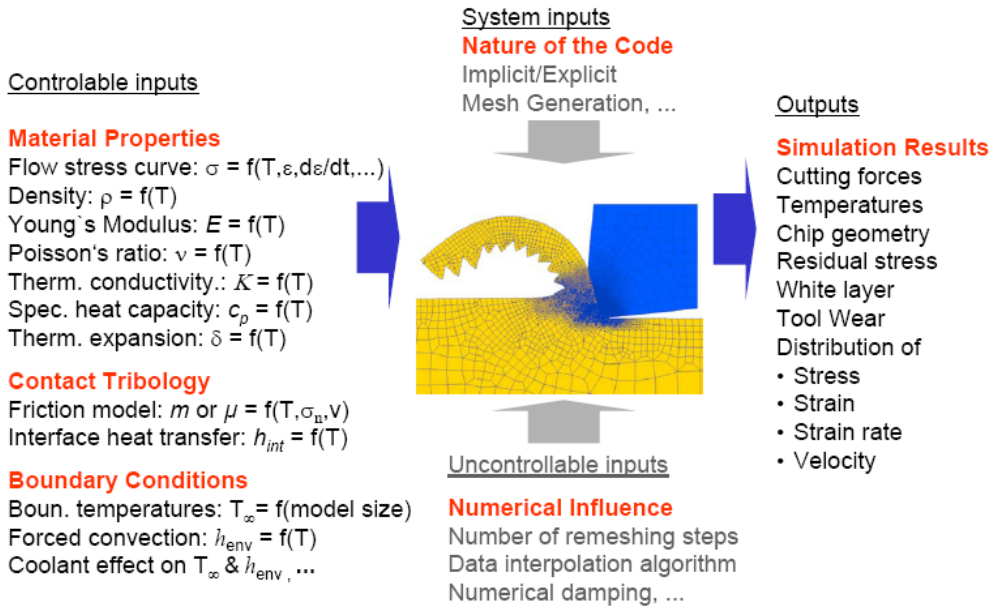

Figure 1.1. Critical input for successful FEM cutting simulation [48].

Despite FEM codes are nowadays widely utilized, there is still a relevant lack of knowledge which remarkably limits their successful application to the design of cutting processes. The most relevant criticisms involve material characterization for strain, strain rate, material hardness and temperature conditions typical of machining, friction data at the tool/part interface, chip formation and heat transfer conditions. All these aspects are detailed in the following paragraphs.

1.3.1 FRICTION AT THE TOOL-CHIP INTERFACE

Friction conditions at the tool-chip interface are very important inputs for modelling and simulation of the machining process.

In machining, the material being removed, i.e. the chip, slides over the tool rake face. The contact region between the chip and the tool is referred to as the tool-chip interface. The nature of the conditions at the tool-chip interface in machining has been the focus of considerable research [43-45]. In the orthogonal cutting process, the chip contact length extends from the cutting edge to a distance where it curls off from the rake face. The heat flowing into the tool is dependent on this contact length with larger contact lengths resulting in the dissipation of more heat into the tool. The other factors that influence the contact length are machining variables, tool and chip geometry, tool and workpiece material, and cutting fluid [46,47].

1.3.2 THERMAL ASPECTS

In machining processes, since heavy deformations are imposed to the material, relevant quantity of heat is generated. In particular, this aspect is becoming very critical in the last years, mainly for two different reasons: the very high cutting speeds, now allowed by the development of new tool materials and powerful machines; and the ever more urgent necessity to reduce or eliminate lubricants and coolants due to the relevant impact on environment and to the heavy influence on the industrial costs [49, 50].

How it is well known, the generated heat is mainly due to the deformation work on the shear plane (primary shear zone), according to many of the traditional models concerning chip formation theory [51].

In addition, a secondary shear zone is located on the rake face, along the contact length. In this area the main responsible of the heat generation is friction between the sliding material and the tool (see Figure 1.2). At the conventional

cutting speeds the largest part of heat is dissipated in the chip and just a low percentage flows towards the tool.

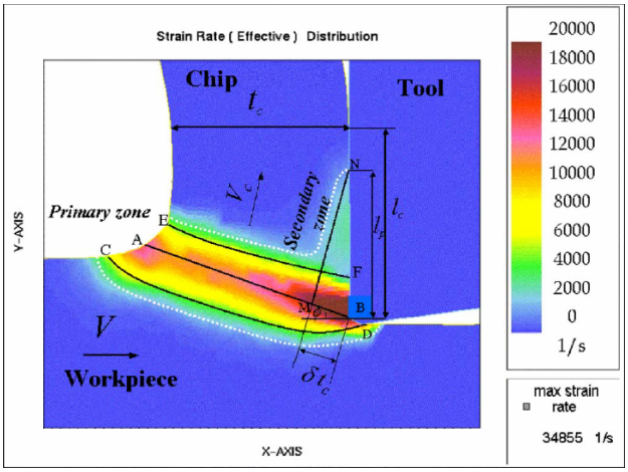

Figure 1.2. Primary and secondary shear zone [60].

According to the above discussed reasons, it is clear that two aspects have to be carefully taken into account as far as heat flux prediction is concerned, namely the evaluation of the global heat transfer coefficient between the chip and the tool and the friction modelling. The former was experimentally calculated by several authors [13, 14], for several couples of material. Nevertheless, many researchers [6,15] attempted to tune this value with the aim to accelerate the convergence of the finite element simulations towards steady state conditions, despite the very short cutting time that can be effectively investigated.

There is another issue to be taken into account: machining simulation can currently investigate only a very short machining time, generally few milliseconds. This time is not sufficient to permit that the heat generated in the primary shear zone arrives to the chip-tool interface and affects the temperature distribution in the tool. Therefore the calculated temperatures in the tool depend mainly on the heat generated by friction in the secondary shear zone and the heat transfer coefficient works, more or less, as a *partitioning* coefficient which determines the heat amounts flowing into the chip and the tool respectively.

According to the above considerations it is worth concluding that an effective, scientifically consistent, numerical analysis of the coupled thermo-mechanical phenomenon is nowadays not yet possible.

1.3.3 MATERIAL FLOW STRESS AT HIGH STRAIN RATE AND TEMPERATURE

One of the most important aspects of the machining modelling by means of finite element simulation is the material modelling of the workpiece material behaviour.

In fact, using FEM based simulation, it is crucial to know the flow stress of the workpiece material under the strain, strain rate and temperature conditions that exist in practical metal cutting operations.

To be useful in metal cutting simulation, flow stress data must be obtained at high strain rates (up to 10^6 s^{-1}), temperatures (up to 1000 $^{\circ}$C) and strains (up to 4) [52].

Previous studies on modelling of material behaviour in the cutting process can be divided into the following categories: rigid-plastic [Iwata et al., 1984; Moriwaki et al., 1993; Ueda and Manabe, 1993), elastic-plastic (Klamecki, 1973; Lajczok, 1980; Usui and Shirakashi, 1982; Strenkowski and Carrol, 1985; Komvopoulos and Erpenbeck, 1991; Zhang and Bagchi, 1994), and viscoplastic (Strenkowski and Carrol, 1986; Strenkowski and Moon, 1990; Joshi et al., 1994). Temperature effects have also been considered in some models, which include thermo-elastic-plastic (Lin and Lin, 1992; Lin and Pan, 1993; Lin and Liu, 1996), thermo-elastic-viscoplastic (Shih and Yang, 1993; Shih, 1995; 1996), and thermo-viscoplastic (Wu et al., 1996; Kim and Sin, 1996) materials.

Nowadays the material properties for metal cutting are obtained mainly using four methods: high-speed compression tests, Hopkinson's bar tests, practical machining tests and reverse engineering using the FEM technique [4,5].

High-speed compression tests [6] are conducted by using compressed air to accelerate a punch and compress a specimen at a very high-speed. The specimen

can be preheated in the furnace before the tests for obtaining material flow stress at elevated temperature. However, the limit of strain rate for this test is in the range of 500 s−1. In addition, the heating rate is considerably lower than that in machining, which causes anneal softening and/or age-hardening of the sample while no such effects have been observed in practical machining [7].

The Hopkinson's bar technique provides faster heat rate by using an induction coil and a higher punch speed. With these improvements, anneal softening and age-hardening are prevented and material data for higher strain rate can be obtained [8]. Modification of sample geometry can raise the achievable strain rate up to 10,000 s−1 for specific materials [9].

Methods to determine the flow stress data through practical machining operations were proposed by different researchers who attempted to approximate the stress, strain, strain rate and temperature conditions that truly exist in machining operations. The data was then directly fitted with a flow stress model. These approaches were addressed in [10–12]. Shatla et al. [2] introduced the inverse mapping method to determine the flow stress instead of curve fitting. This procedure requires less experimental effort. However, the approach was not able to offer a unique solution in all investigated cases.

The FEM technique and experiments have been used together to obtain the flow stress data as presented in [13,14].

CHAPTER 2

FRICTION MODELLING

2.1 INTRODUCTION

During metal cutting, heat is generated both on the shear plane (primary cutting zone) and on the rake face (secondary cutting zone). When the cutting speed is sufficiently high, heat generated on the rake face is the main responsible of the thermal flow through the tool which determines heating and, then, the worsening of the tool mechanical properties leading to wear and, sometimes, breaking.

In this context, a relevant role is played by friction modelling which influences not only the value of the thrust force but also the quota and the distribution of generated heat on the rake face.

On the other hand, even if a proper friction modelling is strongly necessary in order to improve the effectiveness of the simulation of the thermal related phenomena, currently, this topic appears not well-assessed.

In the past several friction models have been proposed but, up to now, it is not established if one of them can be considered as the most effective.

The main objective of the study reported in this chapter, was therefore to assess, if possible, the best friction model, i.e. the one which is able to provide the most effective description of the phenomena involved in the process.

The investigation on the effectiveness of the most diffuse friction models was carried out comparing the numerical predictions with experimental measurements, namely cutting forces, contact length, chip thickness, shear angle and tool temperature.

The analysis was firstly focused on a specific couple workpiece-tool and on the five most commonly used friction models in the simulation of the cutting processes.

Successively, the results obtained from this early stage led to extend the scope of the investigation to further combinations of workpiece-tool materials, including the case of a TiAlN coating.

Finally, the study on the friction modelling in orthogonal cutting was related to an other fundamental aspect of numerical simulation of machining process, namely the flow stress characteristics of the work material.

For this purpose, at the varying of the friction model, four material constitutive equations were implemented in the numerical model and a sensitivity analysis was carried out comparing the numerical predictions and the experimental evidences.

The results of this wide analysis are described in the following paragraphs.

2.2 FRICTION MODELS FOR MACHINING

The attention of the researchers involved in machining field was focused on friction modelling since the beginning of the studies on this process. Over the years several models were proposed all over the world as summarised in the follow.

In early metal cutting analysis, friction conditions at the tool-chip interface were neglected or the simple Coulomb's law was considered on the whole contact zone, using a constant coefficient of friction μ:

$$\tau = \mu \cdot \sigma_n \tag{1}$$

being τ the frictional stress and σ_n the normal one.

Another well known friction model is the constant shear model, which neglects altogether the low stress variation of τ with σ_n. In this case, a constant frictional stress on rake face is assumed, equal to a fixed percentage of the shear flow stress of the working material k:

$$\tau = m \cdot k \tag{2}$$

A more realistic model is related to the actual distribution of stresses on the rake face. The latter is rather complicated and it is typically non linear. According to Zorev [53], the normal stress decreases from the tool edge to the point where the chip separates from the tool. On the contrary, the frictional stress is equal to the shear flow stress near the tool edge and then decreases. According to this distribution the existence of two distinct regions on the rake face was proposed, as shown in Figure 2.1.

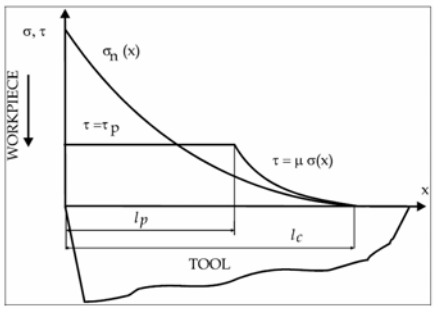

Figure 2.1. Stresses distribution on rake face [Mettere ref].

In the first region, named sticking zone, the normal stress is very large and the frictional stress is assumed to be equal to the shear flow stress of the material being machined. In the latter, on the contrary, the normal stress is small and Coulomb's theory is able to provide a suitable model of the phenomenon.

This can be expressed by means of the following formulation [53]:

$$\begin{aligned} \tau(x) &= \mu \cdot \sigma_n(x) \quad when \quad \tau < k \\ \tau(x) &= k \qquad\qquad when \quad \tau \geq k \end{aligned} \tag{3}$$

Usui and Shirakashi [54] derived an empirical equation as a friction model which relates the frictional stress τ to the normal stress σ_n:

$$\tau = k \cdot \left[1 - e^{-(\mu \cdot \sigma_n / k)}\right] \quad (4)$$

where k is the shear flow stress of the workpiece material and μ is a friction coefficient experimentally obtained for different workpiece-tool material combination.

Childs et al. [55] modified this model by multiplying k with a friction factor m, where 0<m<1:

$$\tau = m \cdot k \cdot \left[1 - e^{-(\mu \cdot \sigma_n / m \cdot k)}\right] \quad (5)$$

It may be verified that for extremely small values of σ_n/k Eq. (5) approaches the (3). The rate of change of τ with σ_n at intermediate levels of σ_n/k may be varied by the further empirical modification of Eq. (6), where n is an exponent that was found ranging between 1 and about 3:

$$\tau = m \cdot k \cdot \left[1 - e^{-(\mu \cdot \sigma_n / m \cdot k)^n}\right]^{\frac{1}{n}} \quad (6)$$

Up to now, no rigorous comparisons between the effectiveness of the proposed models were proposed in literature.

2.3 EXPERIMENTS AND NUMERICAL PREDICTIONS

In order to develop the analysis, an orthogonal cutting experiment was carried out on a lathe, using a tube specimen and an axial feeding (Figure 2.2). The workpiece material was AISI 1045 steel while the cutting tool was an uncoated carbide ISO P30, with a rake angle of 0° and a relief angle of 6°. The tests were executed without any lubricant at the tool-chip interface, with a cutting speed of 100m/min, a feed of 0.1 mm/rev and a depth of cut of 3mm (Case 1).

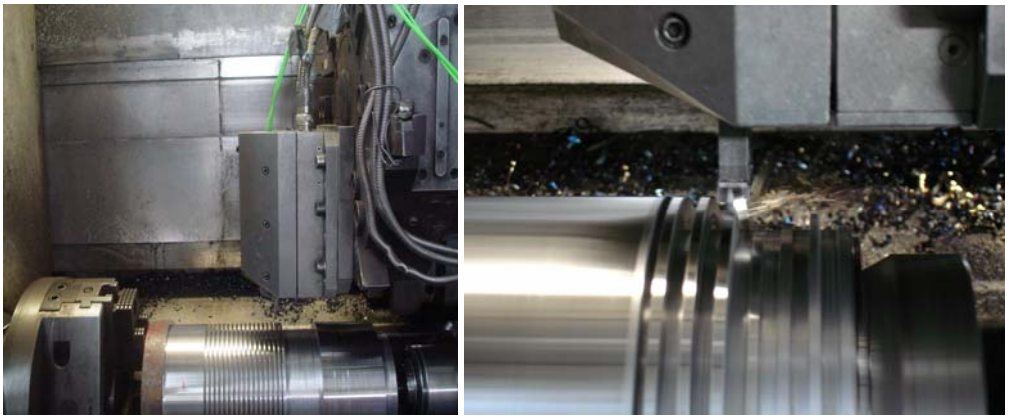

Figure 2.2. Experimental setup.

Cutting and thrust force were measured by using a Kistler piezoelectric dynamometer while a Leica optical microscope was used for estimating both the contact length (Figure 2.3) and chip thickness.

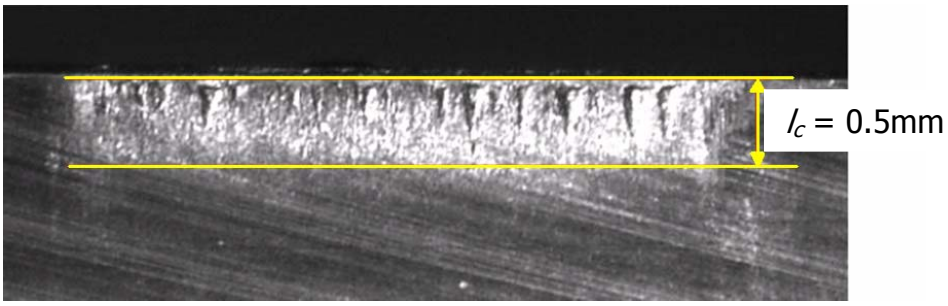

Figure 2.3. The measured contact length by optical microscope.

The temperature was measured using an embedded thermocouple, close to the cutting edge, at a distance of 0.6 mm from the rake face and 0.35 mm from the tool tip (Figure 2.4). Table 2.1 summarizes the experimental results.

As far as the numerical simulations are concerned, the SFTC-Deform-2D code was utilized. It is based on the updated Lagrangian formulation, and an implicit integration method. Since the experiments were carried out in orthogonal cutting conditions, a 2D plane strain simulation was developed in order to reduce the computational time. The workpiece was initially meshed by means of 5000 iso-parametric quadrilateral elements while the tool, modelled as rigid, was meshed into 1000 elements. A coupled thermo-mechanical analysis was carried out.

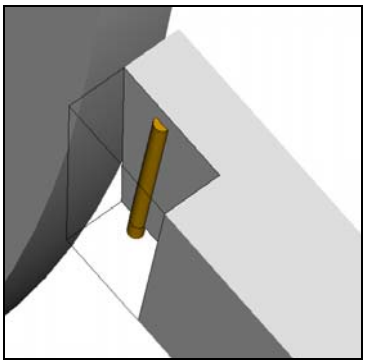

Figure 2.4. Thermocouple position inside the tool.

The material behaviour for the AISI 1045 was described by using a reliable model proposed by Oxley [56]. As far as the friction modelling is concerned, five different formulations were considered according to the above considerations. For each of them, different coefficients were tested obtaining different predictions in order to find the value that better fits the experiments.

No fracture criteria were introduced in the simulation implementing a chip generation strategy based on the remeshing-rezoning algorithm.

Table 2.1. Experimental results.

Cutting force F_c [N]	745
Thrust force F_t [N]	600
Contact length l_c [mm]	0.5
Chip thickness t [mm]	0.29
Shear angle ϕ [deg]	19
Measured temperature [°C]	542

2.3.1 CONSTANT SHEAR FRICTION ON THE WHOLE TOOL-CHIP INTERFACE

A constant shear friction factor was firstly implemented in FE model. Table 2.2 reports the calculated results concerning cutting and thrust force (with the relative errors), contact length, chip thickness and shear angle.

Table 2.2. Constant shear friction on the whole tool-chip interface (model I).

m	F_c [N]	e_{Fc} %	F_t [N]	e_{Ft} %	l_c [mm]	t [mm]	ϕ [deg]
0.30	721	3.2%	328	45.3%	0.17	0.16	30
0.50	706	5.2%	354	41.0%	0.18	0.18	29
0.60	720	3.4%	385	35.8%	0.21	0.18	28
0.65	735	1.3%	405	32.5%	0.19	0.19	27
0.70	743	0.3%	418	30.3%	0.20	0.19	27
0.75	760	2.0%	433	27.8%	0.22	0.19	27
0.80	769	3.2%	449	25.2%	0.25	0.20	26
0.82	780	4.7%	462	23.0%	0.25	0.20	26
0.90	810	8.7%	507	15.5%	0.28	0.21	25

It is interesting to note that a good prediction is obtained as far as the forces are concerned, using an "m" coefficient of about 0.8-0.9. On the other hand, the predicted thrust forces at the reference cutting condition are always lower than experimental force (600 N). A similar discrepancy was observed by Bil et al. [57], although the authors used three different FEM packages. As underlined by Sartkulvanich et al. [58], disagreement of the thrust forces may be due to the difference between the FE model and the actual turning operation. Force measurement in orthogonal turning considers not only the thrust forces from chip formation but also the force that presses the tool upon the workpiece in feed direction. Usually, orthogonal turning tests are conduced either by turning a tube or a disc. These tests do not exactly represent 2D plane strain due to curvature surfaces of the sample and cause force measurements to be different from the predictions. Moreover, it is very inaccurate the evaluation of the contact length, with an error of about 50%. The trend is correct since its tends to increase with friction increasing but the absolute value is not convincing. Probably this poor prediction of the contact length is also due to an accuracy in the experimental measurement. More limited discrepancies are obtained for the deformed chip thickness and shear angle.

2.3.2 CONSTANT COULOMB FRICTION ON THE WHOLE TOOL-CHIP INTERFACE

In this second set of simulations, a constant Coulomb friction factor was fixed on the contact interface between chip and tool. The obtained results are summarized in Table 2.3.

Table 2.3. Constant coulomb friction on the whole tool-chip interface (model II).

μ	F_c [N]	e_{Fc} %	F_t [N]	e_{Fc} %	l_c [mm]	t [mm]	ϕ [deg]
0.1	688	7.7%	322	46.3%	0.27	0.16	29
0.15	708	5.0%	352	41.3%	0.25	0.18	29
0.2	737	1.1%	388	35.3%	0.22	0.18	28
0.25	747	0.3%	408	32.0%	0.21	0.19	27
0.3	752	0.9%	417	30.5%	0.22	0.19	27
0.4	761	2.1%	430	28.3%	0.26	0.20	27
0.5	765	2.7%	442	26.3%	0.24	0.19	27
0.6	772	3.6%	454	24.3%	0.21	0.19	26
0.8	779	4.6%	466	22.3%	0.23	0.20	26

Also in this case the forces data are sufficiently reliable for a value of the friction coefficient that ranges in a wide range. In particular, it is important to underline that the sensitivity to the coefficient changing is very low. Practically coefficients ranging form 0.2 to 0.8 are acceptable.

2.3.3 CONSTANT SHEAR FRICTION IN STICKING REGION AND COULOMB FRICTION IN SLIDING REGION

In the third set of simulations, a constant shear friction factor was imposed in the sticking zone and a Coulomb friction factor was considered in the sliding region. For this purpose, two friction windows were defined in DEFORM. As in Shatla et al. [59], firstly the length of the sticking region was fixed equal to two times the uncut chip thickness. But in this way it was noticed that the sticking region covered all the contact length. Thus, according to other researchers [60] the length of the sticking zone was assumed equal to the uncut chip thickness.

Several friction factors were investigated. The best results were found for the cases reported in Table 2.4.

In this case a slight improvement in the contact length estimation is observed. The condition for which m=0.5 in the sticking zone and μ=0.3 in the sliding one ensures the best trade-off. The forces are well predicted, the contact length is sufficiently well estimated while the deformed chip thickness and shear angle are not satisfactory yet.

Table 2.4. Constant shear friction in sticking region and Coulomb friction in sliding region (model III).

III	F_c [N]	e_c %	F_t [N]	e_t %	lc [mm]	t [mm]	ϕ [deg]
m=0.82 μ= 0.1	737	1.1%	380	36.7%	0.19	0.19	28
m=0.7 μ= 0.2	755	1.3%	424	29.3%	0.23	0.19	27
m=0.6 μ=0.2	741	0.5%	409	31.8%	0.27	0.19	27
m=0.5 μ=0.3	749	0.5%	425	29.2%	0.34	0.19	27
m=0.4 μ=0.3	741	0.5%	428	28.7%	0.22	0.20	27

2.3.4 STICKING-SLIDING MODEL

The fourth set of simulations is based on the model reported in Eq. (3) implemented in the utilised code using a proper designed user-subroutine.

This model again allows a good prediction in cutting force estimation but the evaluation of the thrust force and, especially, contact length, deformed chip thickness and shear angle are not coherent (see Table 2.5).

Table 2.5. Sticking-sliding model (model IV).

IV	F_c [N]	e_c %	F_t [N]	e_t %	lc [mm]	t [mm]	ϕ [deg]
μ=0.2	731	1.9%	387	35.5%	0.26	0.20	28
μ=0.3	742	0.4%	409	31.8%	0.22	0.19	27
μ=0.4	766	2.8%	432	28.0%	0.23	0.20	26

2.3.5 VARIABLE SHEAR FRICTION ON THE TOOL-CHIP INTERFACE

A variable shear friction stress on the tool-chip interface was considered as a function of the normal pressure. It was calculated on the basis of the model proposed in Eq. 6 where the coefficients m, μ and n were chosen according to Dirikolu et al. [61]. The results for the best case are reported in Table 2.6.

Table 2.6. Variable shear friction at the entire tool-chip interface (model V).

F_c [N]	e_c %	F_t [N]	e_t %	l_c [mm]	t [N]	ϕ [deg]
755	1.3%	432	28.0%	0.22	0.20	27

Analyzing the data in the table, it is possible to assess that model V supplies results comparable to the other models. A good prediction of the forces does not correspond to a good prediction of the other mechanical variables that show errors of about 50%.

2.3.6 BEST RESULTS FOR EACH PROPOSED MODEL

Taking into account the experimental data, for each one of the proposed models the best trade-off among the tested parameters were determined, as shown in Table 2.7.

Table 2.7. Best results for each friction model.

MODELS	F_c [N]	F_t [N]	l_c [mm]	t [mm]	ϕ [deg]
I (m=0.82)	780	462	0.25	0.20	26
II (μ=0.4)	761	430	0.26	0.20	27
III (m=0.5; μ=0.3)	749	425	0.34	0.19	27
IV (μ=0.2)	731	387	0.26	0.20	28
IV (μ=0.4)	766	432	0.23	0.20	26
V	755	432	0.22	0.20	27

These results demonstrate that the different formulations do not provide substantial differences as far as the "mechanical results" are concerned.

Based on this consideration, the following step was to verify the thermal behaviour of the different models since comparable results can be obtained properly setting the constants if the mechanical issues are taken into account.

2.3.7 ON THE TEMPERATURE IN THE TOOL

Despite at the varying of the friction model the sensitivity is very low as far as the mechanical variables are regarded, it is very interesting to observe how the situation completely changes if thermal issues are investigated.

A thermal analysis was also carried out taking into account the different friction models. It is well known that in thermo-mechanical simulation of metal cutting a very short process time can be effectively simulated. During this limited time, many process variables do not reach steady state conditions. Among these the temperature surely plays a relevant role in the occurrence (and modeling) of different process phenomena. Anyway, a punctual prediction of the thermal aspects is allowed in the thermo-mechanical simulation only if particular procedures are implemented.

Some researchers, for instance, artificially increase the global thermal exchange coefficient. In fact, it was demonstrated that high values of h [62] allow to reach steady state temperatures in a very short time of simulation. In this way the thermal equilibrium is suddenly reached at the tool-chip interface but the temperature distribution, for instance in the tool, is quite different respect to the real one. Therefore, this procedure results more a trick than a rigorous scientific approach, thus this issue has to be accurately investigated. Besides an important factor to take into account is the friction modeling at the chip-tool interface because it is the main cause of energy generation in the thermo-mechanical analysis.

In the present study it was studied the variation of the temperature distribution in the tool when the different friction models are adopted.

An inverse approach was utilized to evaluate the global film coefficient h. More in detail, the procedure for each friction model was the following:

1. a 2D thermo-mechanical numerical simulation was run imposing a global heat transfer coefficient equal to 1000 kW/m^2K. In fact, how it was pointed out by Filice et al. [63], a value of h close to 1000 kW/m^2K permits a satisfactory agreement between the numerical data and the experimental evidences;

2. when the temperatures at the tool-chip interface reached the steady-state conditions, the simulation was stopped and the nodal temperatures on rake face were collected;

3. the obtained nodal temperatures of 2D analysis were then applied as boundary conditions for a subsequent 3D Eulerian thermal analysis;

4. the steady-state temperature were previously experimentally measured by using a proper thermocouple placed in the tool, then the error between the predicted and the experimental temperatures was calculated:

4.1 if the error was lower than an acceptable value (5%) then global interface film coefficient, h, was found;

4.2 else, return to step 1 and increase or decrease global interface heat transfer coefficient, h, according to the obtained error.

Having a look at the Table 2.8, it is possible to state that only in four cases the proposed procedure converged, allowing to calculate the temperature in the tool with an acceptable error.

Thus, the friction model heavily affects the thermal result.

More in details, even if this part of the study was focused only on one material and one process configuration, it is important to highlight that apart from small differences, the main mechanical results (i.e. forces, contact length and so on) appears practically not sensitive to friction model. On the contrary, friction becomes probably the most relevant issue in thermal analysis since it determines the rake face heating.

Table 2.8. Predicted temperature in the tool.

MODELS	h [kW/m^{2}K]	T_{FEM} [°C]	e %
I (m=0.82)	1000	560	3.32%
II (μ=0.4)	10000	551	1.67%
III (m=0.5; μ=0.3)	1000000	324	40.22%
IV (μ=0.2)	10000	443	18.27%
IV (μ=0.4)	10000	551	1.67%
V	100	545	0.55%

Taking into account this considerations the study was successively extended in order to take into account other couples of workpiece-tool, different cutting conditions and other material laws.

All these aspects will be discussed in the next paragraphs.

2.4 DIFFERENT COUPLES TOOL-WORKPIECE

With the aim of enlarging the investigation on the role played by the implemented friction model within a 2D simulation of orthogonal cutting, the initial experimental campaign was enhanced with new orthogonal cutting experiments.

The new workpiece-tool materials utilized were:

AISI 1020 - uncoated carbide ISO P25 tool (Case 2),

AISI 1045 - uncoated carbide ISO P40 (Case 3),

AISI 1045 - carbide ISO P40 with a TiAlN coating (Case 4).

All the turning tests were carried out using a feed of 0.1 mm/rev and a cutting speeds of 100 m/min. The depth of cut was generally 3 mm but it was fixed equal to 2.5 mm in the Case 2. The rake angle was equal to 0°C in the Case 2, while it was equal to +10° in the other ones.

All the measurements were executed utilizing the same procedure described in the paragraph 2.3. Therefore, cutting and thrust forces were measured by using a

piezoelectric dynamometer while an optical microscope was used for estimating both the chip contact length and chip thickness. Temperatures were measured using a single wire thermocouple that was directly embedded in the tool, at a know distance from the rake face (about 0.35 mm). Table 2.9 summarizes the experimental results in terms of cutting and thrust forces, chip contact length, chip thickness and measured temperature for both the old case and the new cases.

Table 2.9. Experimental results.

Measured parameters	CASE 1	CASE 2	CASE 3	CASE 4
Cutting force F_c [N]	745	920	820	710
Thrust force F_t [N]	600	463	620	386
Contact length l_c [mm]	0.5	0.529	0.36	0.28
Chip thickness t [mm]	0.29	0.42	0.28	0.21
Temperature [°C]	542	483	514	417

Data in Table 2.9 were calculated as average value of 5 measures for each configuration.

In this investigation, for a second time the finite element code DEFORM-2D, was used to simulate the cutting process. For all the cases the workpiece was modelled as elastic-plastic and the tool as rigid, and 2D plane strain conditions were imposed in the simulation. Also this time the material flow stress model proposed by Oxley [56] was used in finite element code, for both AISI 1020 and AISI 1045 materials.

The investigation was restricted to the three most common friction models, namely the constant shear friction on the tool-chip interface (model I), the constant Coulomb friction on the whole tool-chip interface (model II) and finally the sticking-sliding model (model IV). The motivation is the very broad employment of these models among the experts in the field. In addition, analysing the results obtained by using the other two models (model III and model V), it was observed that they do not provide a better prediction of the mechanical variables. Moreover both model III and model V present an important difficulty: in the first case (model III) it is necessary to fix the length of the sticking region,

while in the second case (model V) it is necessary to know the shear flow stress of the material.

The study, taking into account the results of the previous analysis, was also restricted in terms of friction coefficients.

Tables from 2.10 to 2.12 summarize the best numerical results for all the investigated cases concerning cutting and thrust forces, chip contact length and chip thickness. The Tables also report the relative errors for each parameter and the average error $\bar{e}$.

Table 2.10. Best numerical results for each friction model (Case 2).

Model	F_c [N]	e_{Fc} %	F_t [N]	e_{Ft} %	l_c [mm]	e_{lc} %	t [mm]	e_t %	$\bar{e}$ %
I (m=0.85)	864	6.1	545	17.7	0.55	4.0	0.32	23.8	12.90
II (μ=0.90)	839	8.8	499	7.8	0.38	28.2	0.30	28.6	18.35
III (μ=0.90)	843	8.4	501	8.2	0.34	35.7	0.31	26.2	19.63

Table 2.11. Best numerical results for each friction model (Case 3).

Model	F_c [N]	e_{Fc} %	F_t [N]	e_{Ft} %	l_c [mm]	e_{lc} %	T [mm]	e_t %	$\bar{e}$ %
I (m=1.00)	747	8.9	361	41.8	0.26	27.8	0.21	25.0	25.88
II (μ=0.85)	654	20.2	240	61.3	0.18	50.0	0.18	35.7	41.80
III (μ=0.80)	667	18.7	257	58.5	0.16	55.6	0.18	35.7	42.13

Analyzing each couple of materials it is possible to state that the different friction formulations do not provide very relevant differences as far as the mechanical parameters are concerned. On the other hand, taking into account all

Table 2.12. Best numerical results for each friction model (Case 4).

Model	F_c [N]	e_{Fc} %	F_t [N]	e_{Ft} %	l_c [mm]	e_{lc} %	t [mm]	e_t %	$\bar{e}$ %
I (m=0.80)	762	7.3	417	8.0	0.20	28.6	0.18	14.3	14.55
II (μ=0.80)	760	7.0	433	12.2	0.26	7.1	0.19	9.5	8.95
III (μ=0.90)	747	5.2	431	11.7	0.24	14.3	0.19	9.5	10.18

the cases it is possible to highlight that a proper friction model and coefficient has to be selected for each specific workpiece-tool system. The best model and

coefficient for each of the investigated case is reported in Table 2.13, taking into account also the first couple workpiece-tool investigated.

Table 2.13. Best Results for each couple of materials.

Couple	Model	F_c [N]	e_{Fc} %	F_t [N]	e_{Ft} %	l_c [mm]	e_{lc} %	t [mm]	e_t %	$\bar{e}$ %
1	I (m=0.90)	810	8.7	507	15.5	0.28	44.0	0.21	27.6	23.95
2	I (m=0.85)	864	6.1	545	17.7	0.55	4.0	0.32	23.8	12.90
3	I (m=1.00)	747	8.9	361	41.8	0.26	27.8	0.21	25.0	25.88
4	II (μ=0.80)	760	7.0	433	12.2	0.26	7.1	0.19	9.5	8.95

Several considerations may be developed on the data of Table 2.13; from a practical point of view, it is possible to state that all the models are able to provide sufficient predictions, also because average errors of 10-20% have to be considered as acceptable in this field. What is more, the most relevant error is caused on the contact length, probably due to the not very accurate mesh refining at the chip-rake face interface. In general, taking into account the available data, the use of Model I, setting a shear factor in the range 0.80-1.00, constitutes a good approach for friction modelling in the investigated cases. In the Case 4, in fact, Model II is the best only taking into account chip contact length.

2.4.1 TEMPERATURE ESTIMATION

Also this time a thermal analysis was carried out . In order to overcome the problem related to the possibility of simulating only few milliseconds of the machining process time, the strategy based on an artificial increasing of the global heat transfer coefficient h between the tool and workpiece was adopted. In particular, as in the previous analysis, a value of h close to 1000 kW/m^{2}K was utilized, since it permitted [63] a satisfactory agreement between the numerical data and the experimental evidences, for a specific couple workpiece-tool (AISI 1045 – ISO P20). The procedure utilized was the same as in the paragraph 2.3.7.

More in detail, the influence of the friction model on temperatures was investigated for the Cases 1 and 2, using the *best* coefficients for each model, according to the above reported results.

Data provided by the simulations are summarized in Table 2.14.

Table 2.14. Predicted Temperature in the Tool.

CASE 1 MODELS	T_{FEM} [°C]	e%	CASE 2 MODELS	T_{FEM} [°C]	e%
I (m=0.90)	560	3.32%	I (m=0.85)	535	10.33%
II (μ=0.40)	555	2.40%	II (μ=0.90)	739	53.00%
III (μ=0.40)	565	4.24%	III (μ=0.90)	670	38.72%

It can be observed that the numerical temperatures are strictly dependent on the friction model and on the selected constants. This is consistent with theory since a relevant quota of heat is generated in the secondary shear zone. However, the sensitivity of temperature on the friction model and coefficient is very high and all the simulations are influenced by the choice of the *h* value. It seems clear that, while the mechanical variables can be estimated properly setting the friction model, further efforts are required as far as the thermal aspects are regarded.

In fact, also the strategy to increase the global heat transfer coefficient is not completely physically consistent, even if it permits to obtain a quicker reaching of thermal steady state.

Furthermore, it is possible to state that a generally applicable model is not yet available as regards the thermal simulation.

On the other hand , since a proper friction model and coefficient have to be selected for each specific workpiece-tool system, the analysis was extended to the study of friction related to material modelling as shown in the following sections of this chapter.

2.5 DEPENDENCE OF MACHINING SIMULATION EFFECTIVENESS ON MATERIAL AND FRICTION MODELLING

As already announced, the initial analysis of the friction modelling in the numerical simulation of cutting processes, was extended in order to obtain a

deeper understanding of the aspects involved. With this aim, the couple workpiece – tool was fixed, as well as the heat transfer coefficient at tool - chip interface, while different cutting conditions were taken into account. In addition, the attention was focused on the effects of different combination of friction models and material laws, utilized to describe the workpiece material behaviour.

Several researches were focused on the effects of flow stress and friction models in finite element simulation. Childs [64] utilized several flow stress laws, proposed in the literature, with the aim of analyzing their effects on the prediction of process mechanics in the primary and the secondary shear zones. He found that, despite the differences existing in their structure, the material laws provided similar numerical flow stress values in the primary shear zone, but caused large differences in the secondary shear zone. According to the author, this discrepancy was mainly due to the friction law since machining has very severe friction conditions and small changes in friction modelling can cause large changes in chip formation.

The above conclusions were confirmed by Ozel [60]. In particular, he found that machining modelling is greatly influenced by two major factors: a) flow stress characteristics of the work material, and b) friction characteristics at the tool-chip interface. However, in the analysis, he took into account only the influence of the friction law.

A sensitivity analysis of the influence of flow stress and friction laws was recently proposed by Sartkulvanich et al. [58] even if their study was more oriented on the flow stress aspects. Furthermore, they utilized a power law obtained by fitting the data from Hopkinson's bar tests, and two friction laws were utilized in their investigation.

Recently, Childs and Rahmad [65] recognized that a complete analysis requires one to take into account the effects of the flow stress and of the friction law at the tool-chip interface. However, their study was oriented on a sensitivity analysis of the strain-hardening data on the main cutting variables (cutting force and thrust force) using several FE codes.

According to the state of the art, it is evident that there is a necessity to carry out a wider analysis aimed at investigating the influence of both material flow stress laws and friction models on the effectiveness of FE simulations of cutting processes.

This is the objective of this study, which is focused, for sake of simplicity, on the simulation of an orthogonal cutting process of a plain-carbon steel (AISI 1045) utilizing different material laws and friction models. Four rheological models were considered for the material, as well as three different friction laws. For each law, several friction coefficients were used generating a very extensive plan of finite element simulations, which constitutes the knowledge base of this research. The different mechanical variables predicted using numerical simulations were compared with the experimental results.

2.5.1 EXPERIMENTAL TESTS AND NUMERICAL SIMULATIONS

An experimental investigation was carried out in order to acquire the necessary data to validate the numerical predictions. In particular, a few cutting tests were run on a lathe, reproducing orthogonal cutting conditions.

The workpiece material was AISI 1045 steel, while the cutting tool was an uncoated carbide ISO P30, with a rake angle of 0°, a relief angle of 6°, and an edge radius of 0.05 mm. The width of cut was 3mm. The tests were executed without any lubricant at the tool–chip interface, utilizing the values of cutting speed and feed rate reported in Table 2.15. All the experiments were repeated three times, showing an uncertainty of ± 6-10% (95% confidence interval).

Table 2.15. Cutting conditions.

CASE	Cutting Speed (m/min)	Feed Rate (mm/rev)
1	100	0.1
5	150	0.1
6	100	0.15

Different mechanical variables were detected during the tests. Cutting and thrust forces were measured by using a piezoelectric dynamometer, while an optical microscope was used to estimate both the chip contact length and chip thickness. Table 2.16 shows the average experimental results of cutting and thrust forces, chip contact length, chip thickness and shear angle.

Table 2.16. Experimental results.

TEST CASE	1	5	6
Cutting force F_z [N]	745	715	1027
Thrust force F_t [N]	600	522	749
Contact length l_c [mm]	0.50	0.53	0.60
Chip thickness t [mm]	0.288	0.220	0.355
Shear angle ϕ [deg]	19.0	24.4	23.0

In this investigation, the finite element code SFTC-Deform-2D was utilised [66]. The workpiece, modelled as rigid-plastic, was initially meshed by means of 3000 iso-parametric quadrilateral elements while the tool, modelled as a rigid body, was meshed into 1000 elements (Figure 2.5). It is worth pointing out that the global heat transfer coefficient at the tool-chip interface, h, was fixed equal to 1000 kW/m^{2}K taking into account some previous studies [67].

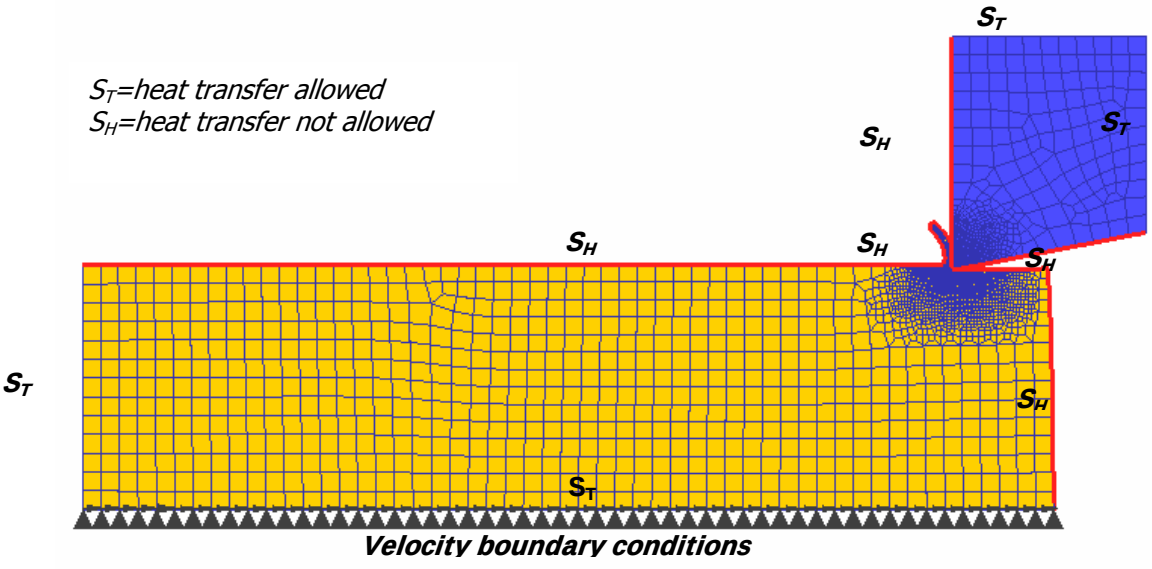

Figure 2.5. FE model and scheme of initial boundary conditions.

2.5.2 MATERIAL AND FRICTION MODELLING

As mentioned, four different constitutive models were tested in order to model the plastic behaviour of AISI 1045 steel.

The first one (indicated as M1) is the model originally proposed by Oxley [56]; the effective flow stress is computed as an exponential function of the effective strain ε:

$$\sigma = \sigma_1 \varepsilon^{n_1} \tag{7}$$

with σ_1 being the strength coefficient and n_1 the strain-hardening exponent. Both σ_1 and n_1 are considered as functions of the parameter velocity-modified temperature, T_{mod}, which includes the effects of strain rate, $\dot{\varepsilon}$, and temperature , T_1. The velocity-modified temperature parameter was proposed by McGregor and Fisher [68] and is defined as:

$$T_{\mathrm{mod}} = T_1 \cdot \left(1 - \nu \log \frac{\dot{\varepsilon}}{\dot{\varepsilon}_0} \right) \tag{8}$$

where ν and $\dot{\varepsilon}_0$ are constants depending on the workpiece material, available in [56]. The relationships σ_1 vs. T_{mod} and n_1 vs. T_{mod} have been experimentally established using high speed compression tests [56].

The second utilized flow stress equation is the well known Johnson-Cook model [69] (indicated as M2):

$$\sigma = \left(A + B\varepsilon^n\right) \cdot \left(1 + C \ln\left(\frac{\dot{\varepsilon}}{\dot{\varepsilon}_0} \right) \right) \cdot \left(1 - \left(\frac{T - T_{room}}{T_{melt} - T_{room}} \right)^m \right) \tag{9}$$

where σ is the stress (MPa), ε the strain, $\dot{\varepsilon}$ the strain rate (s^{-1}), $\dot{\varepsilon}_0$ the reference strain rate (s^{-1}), and *A*, *B*, *C*, *n*, *m* are the material flow stress parameters.

In particular, the J-C material constants in model M2 were identified through high strain rate mechanical testing using the Split Hopkinson's Pressure Bar

method under a constant strain rate of 7500 s^{-1} within the temperature range 20-700°C. The constants utilized here were found by Jaspers and Dautzenberg [70].

The third utilized model (indicated as M3) was developed by Sartkulvanich et al. [52] and it is a modified Johnson-Cook model. The flow stress equation is given by:

$$\sigma = \left(B\varepsilon^{n}\right)\cdot\left(1+C\ln\left(\frac{\dot{\varepsilon}}{\dot{\varepsilon}_{0}}\right)\right)\cdot\left(\left(\frac{T_{room}-T}{T_{melt}-T_{room}}\right)+ae^{-0.0005(T-700)^{2}}\right) \tag{10}$$

where σ, ε, $\dot{\varepsilon}$ and $\dot{\varepsilon}_{0}$ have the same meaning as in the Johnson-Cook model mentioned above, and *B*, *C* and *a* are the redefined material flow stress parameters.

The modified J-C material constants proposed by Sartkulvanich et al. [52] (model M3) for AISI 1045 were determined using a methodology (namely OXCUT) based on analytical modelling of the orthogonal slot milling process. It is worth recognizing that the ranges of strain rate, true strain and temperature regimes are not reported in Sartkulvanich et al. [52].

Finally, an empirical model (indicated as M4) developed by Usui et al. [71], based on the Split Hopkinson Bar hot compression test, was implemented. The full expression for flow stress, including strain path effects, is:

$$\sigma = A\cdot\left(\frac{\dot{\varepsilon}}{1000}\right)\cdot e^{aT}\left(\frac{\dot{\varepsilon}}{1000}\right)\cdot\left(\int_{strain\_path} e^{-aT/N}\left(\frac{\dot{\varepsilon}}{1000}\right)^{-m/N} d\varepsilon\right)^{N} \tag{11}$$

When straining takes place at constant strain rate and temperature, it reduces to:

$$\sigma = A\cdot\left(\frac{\dot{\varepsilon}}{1000}\right)^{M}\cdot\varepsilon^{N} \tag{12}$$

where *A*, *M* and *N* depend on temperature. The form of model M4 that was used in this work utilized the simplified form provided in eq.6.

The material constants were identified for a temperature range from 20°C to 720°C, strain rate up to 2000 s^{-1} and true plastic strain up to 1.

It is important to underline that the described flow stress models show different responses even when they are referred to the same workpiece material, as shown in Figure 2.6.

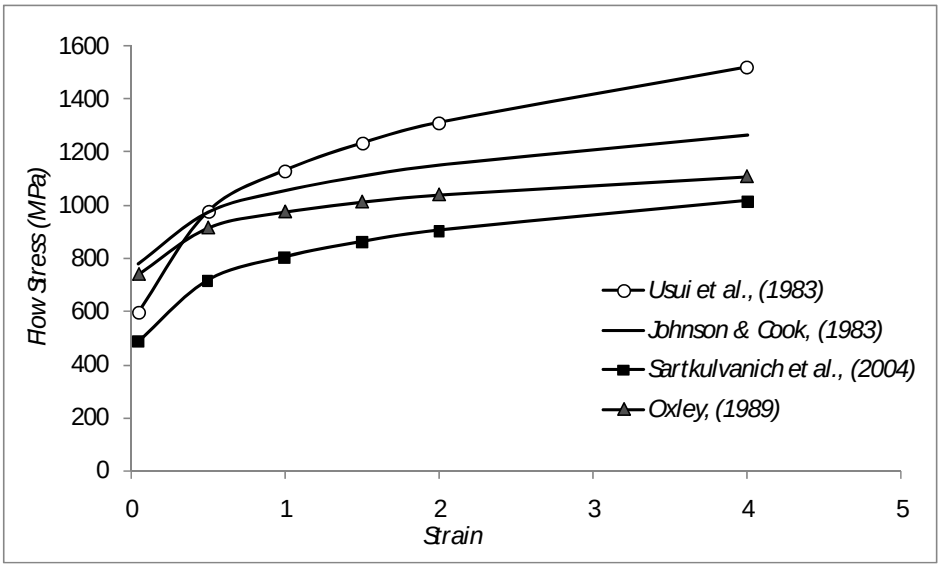

Figure 2.6. Flow stress response for temperature 300°C and strain rate 1000s^{-1}.

As far as friction modelling is concerned, the three most common friction models for machining processes were taken into account in this study. These models, already described in this Chapter (Paragraph 2.2), are respectively the constant shear model (Equation 2 – model I), the Constant Coulomb model (Equation 1 – model II) and finally the sticking-sliding model (Equation 3 – model IV).

In order to investigate the sensitivity of the predicted variables to the friction model used, different coefficients were utilized according to Table 2.17. All the above models can be easily implemented in the chosen FE code.

Table 2.17. Utilized friction coefficients

Friction Model	Friction Coefficient
Constant shear	0.2; 0.4; 0.6; 0.82
Constant Coulomb	0.2; 0.4; 0.6
Sticking-sliding	0.1; 0.2; 0.4

2.5.3 NUMERICAL RESULTS

2.5.3.1 FORCE PREDICTIONS USING THE CONSTANT SHEAR MODEL

First of all, the material flow stress models were compared taking into account the predictions of the cutting and thrust forces they provide. For this stage of the research, the constant shear model was fixed as the friction model.

Figures 2.7, 2.8 and 2.9 show that the most effective predictions (i.e., the closest ones to the experimental data) are given by the material model M1 [56], utilizing the highest friction factor (m = 0.82). For this combination of material model and friction factor, the average error is very low as far as the principal cutting force, F_z, is concerned and the error in the thrust force prediction, F_t, is also acceptable (more or less 20%). Similar results are also provided by the M3 model [52] for prediction of thrust force. The errors obtained in prediction of forces utilizing the other models are significantly higher, particularly for thrust force.

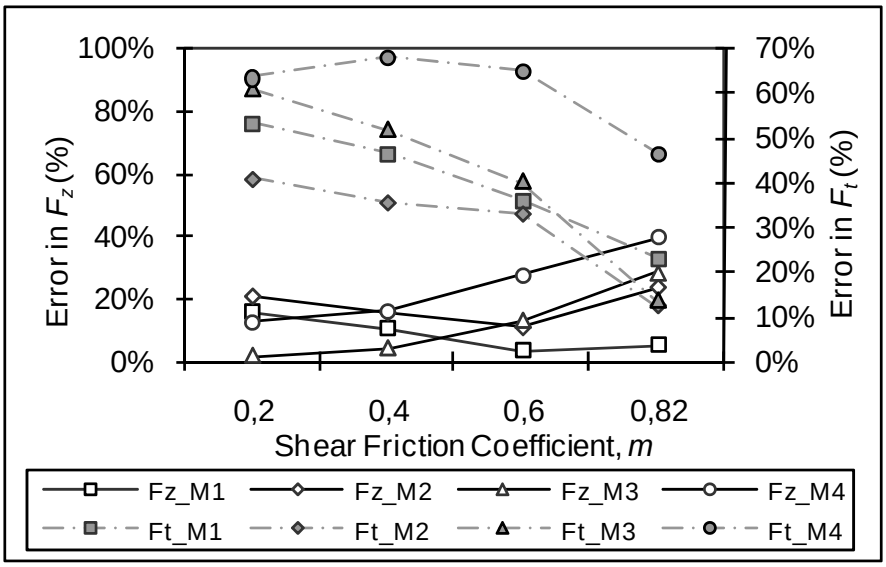

Figure 2.7. Percentage errors for cutting and thrust forces using the constant shear model (V_c = 100 m/min, f = 0.1 mm/rev).

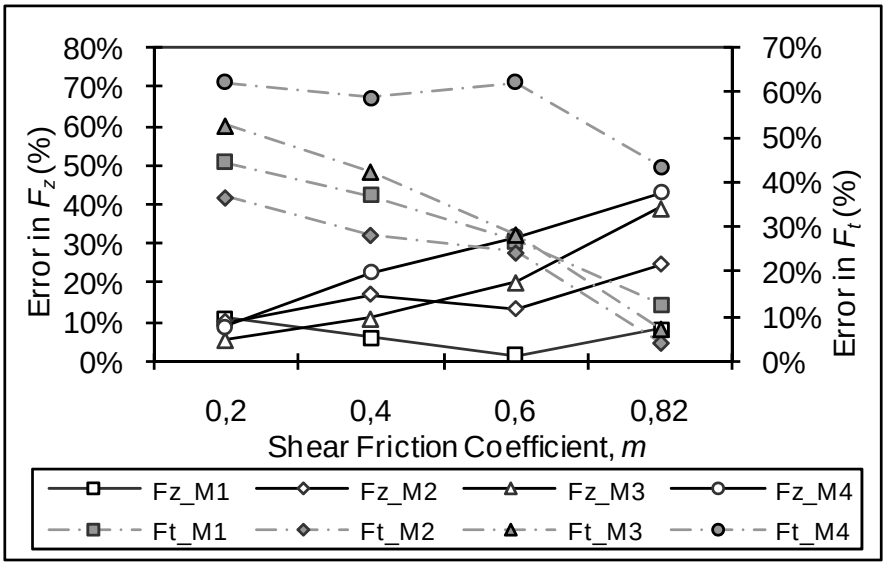

Figure 2.8. Percentage errors for cutting and thrust forces using the constant shear model (V_c = 150 m/min, f = 0.1 mm/rev).

2.5.3.2 FORCE PREDICTIONS USING THE COULOMB MODEL

Material model M1 still gives the lowest error when utilizing Coulomb's friction model instead of the constant shear one (Figures 2.10, 2.11 and 2.12) as far as the principal cutting force (F_z) is concerned. For this model, the best predictions are obtained using the lowest friction coefficient (μ = 0.2) at all test conditions. It is also interesting to note that the sensitivity of principal cutting force (F_z) on the friction coefficient is relatively low.

In contrast, the errors in predictions of thrust force (F_t), in general tend to decrease with increasing friction coefficient, and these effects are more evident when higher cutting speed (Figure 2.11) and feed rate (Figure 2.12) are utilized. Furthermore, if only the thrust force (F_t) needs to be predicted within an acceptable error, then the material models to use in the numerical analysis are M2 or M3, in combination with the highest friction coefficient (μ = 0.6).

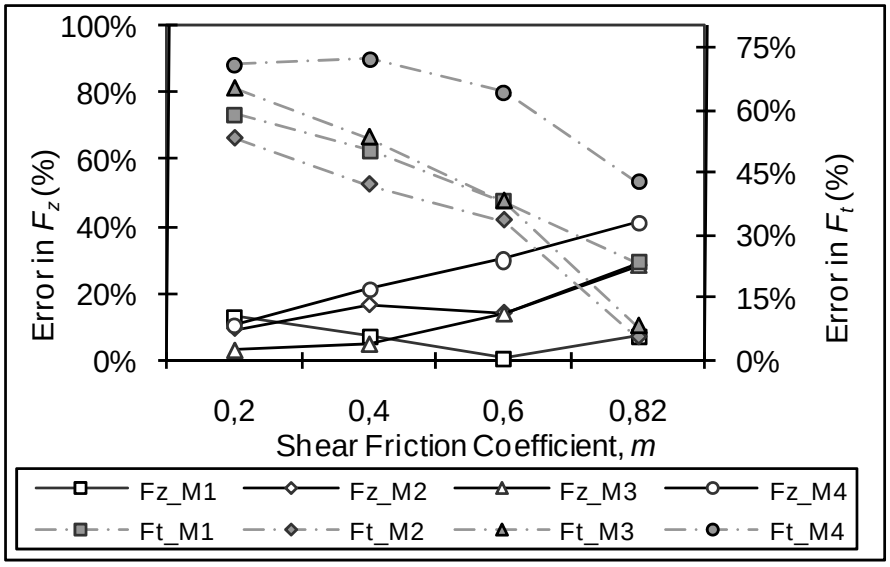

Figure 2.9. Percentage errors for cutting and thrust forces using the constant shear model (V_c = 100 m/min, f = 0.15 mm/rev).

2.5.3.3 FORCE PREDICTIONS USING THE STICKING-SLIDING MODEL

As far as the principal cutting force (F_z) is concerned, the best predictions are given by material model M1 when a friction coefficient is larger than 0.2, or by model M3 for a friction coefficient equal to 0.1 (Figures 2.13, 2.14 and 2.15).

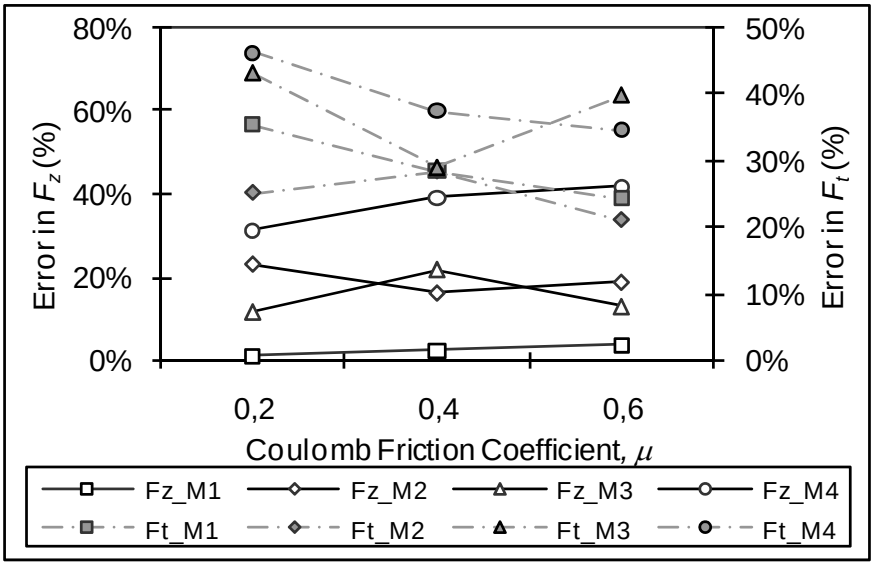

Figure 2.10. Percentage errors for cutting and thrust forces using the constant coulomb model (V_c = 100 m/min, f = 0.1 mm/rev).

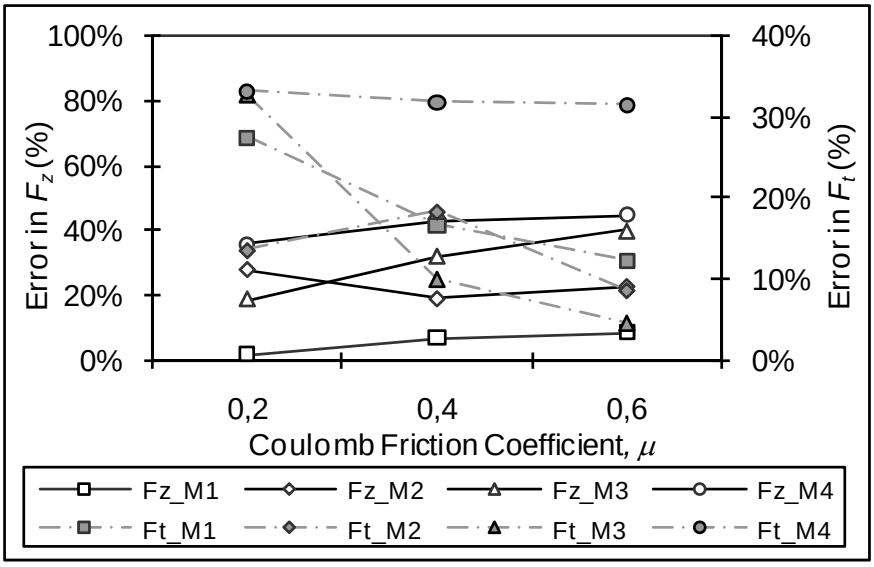

Figure 2.11. Percentage errors for cutting and thrust forces using the constant coulomb model (V_c = 150 m/min, f = 0.1 mm/rev).

However, larger friction coefficients are necessary in order to improve the numerical prediction on thrust force (F_t) when sticking-sliding model is used, as shown in Figures 2.13, 2.14 and 2.15. As already observed for the Coulomb friction model, the best predictions of thrust force (F_t) are given, in general, by material model M3, in particular at higher cutting speed (Figure 2.14).

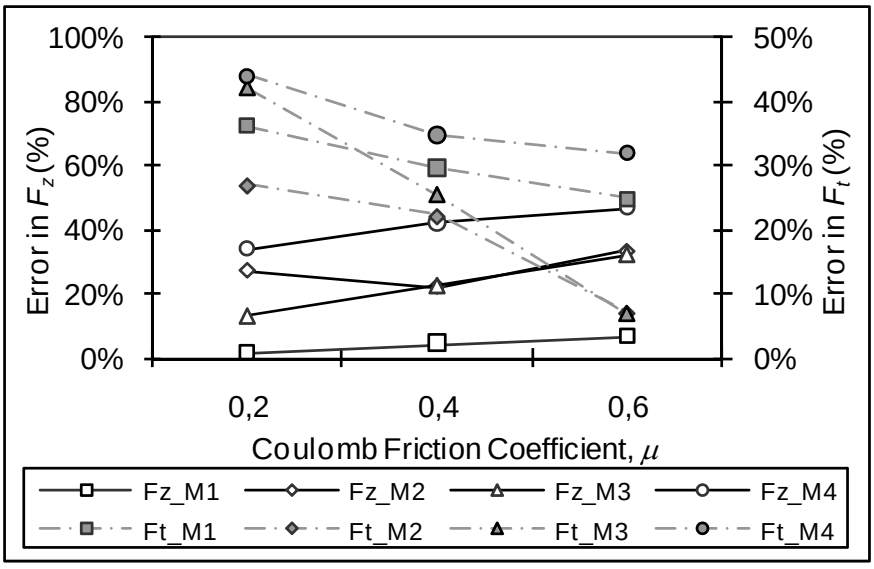

Figure 2.12. Percentage errors for cutting and thrust forces using the constant coulomb model (V_c = 100 m/min, f = 0.15 mm/rev).

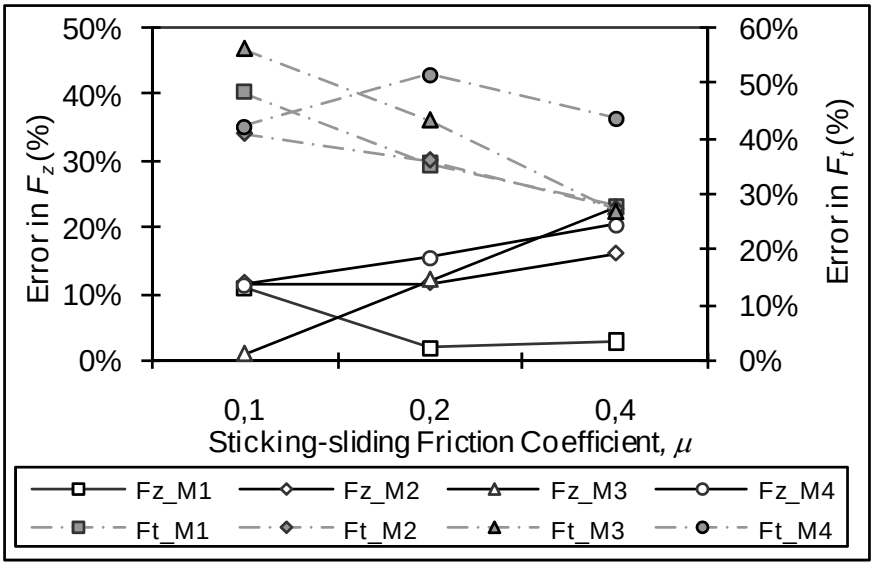

Figure 2.13. Percentage errors for cutting and thrust forces using the sticking-sliding model (V_c = 100 m/min, f = 0.1 mm/rev).

2.5.3.4 CUTTING CONTACT LENGTH AND SHEAR ANGLE PREDICTIONS USING THE CONSTANT SHEAR MODEL

Of course, limiting the study only to prediction of forces would present a partial picture.

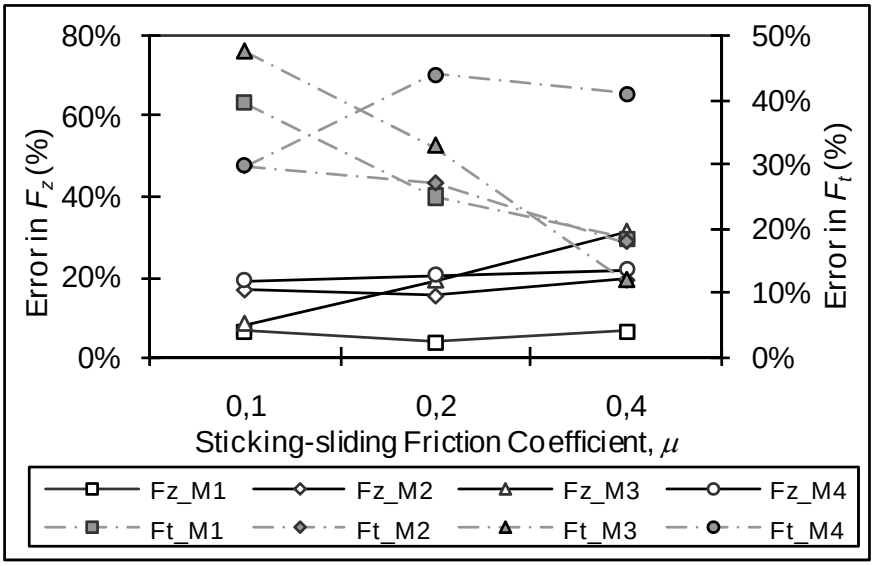

Figure 2.14. Percentage errors for cutting and thrust forces using the sticking-sliding model (V_c = 150 m/min, f = 0.1 mm/rev).

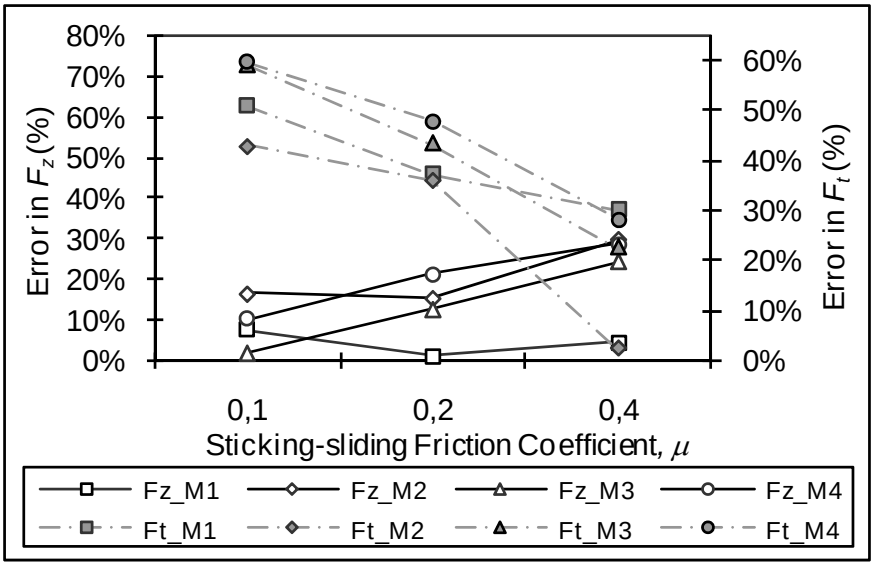

Figure 2.15. Percentage errors for cutting and thrust forces using the sticking-sliding model (V_c = 100 m/min, f = 0.15 mm/rev).

Therefore, for sake of completeness, a higher number of mechanical variables were investigated: the shear angle, ϕ, and the cutting contact length, l_c, were also introduced. The principle is that a reliable simulation has to properly predict the highest number of variables.

As far as the shear angle, ϕ, is concerned, all the four utilized constitutive models show similar trends: the percentage errors decrease with increasing friction coefficient (Figures 2.16, 2.17 and 2.18). What is new in this case is that the lowest error predictions are given by material model M4 [71] and these errors are lower when higher cutting speed (Figure 2.17) and feed rate (Figure 2.18) are utilized. In contrast, the errors in predictions given by model M1 are generally larger than 25%.

As far as the cutting contact length, l_c, is concerned, it can be observed in Figures 2.16, 2.17 and 2.18 that the errors between predicted and measured values become lower when higher friction coefficients are utilized. In addition, the best trade-off seems to be given again by model M4. Model M3 also shows acceptably low errors. It is worth pointing out that when the contact length, l_c, is investigated, a relatively large scatter is present in the predicted values.

Actually, the contact length prediction is always affected by a relatively high error and, unfortunately, this is a typical condition in numerical simulation of cutting.

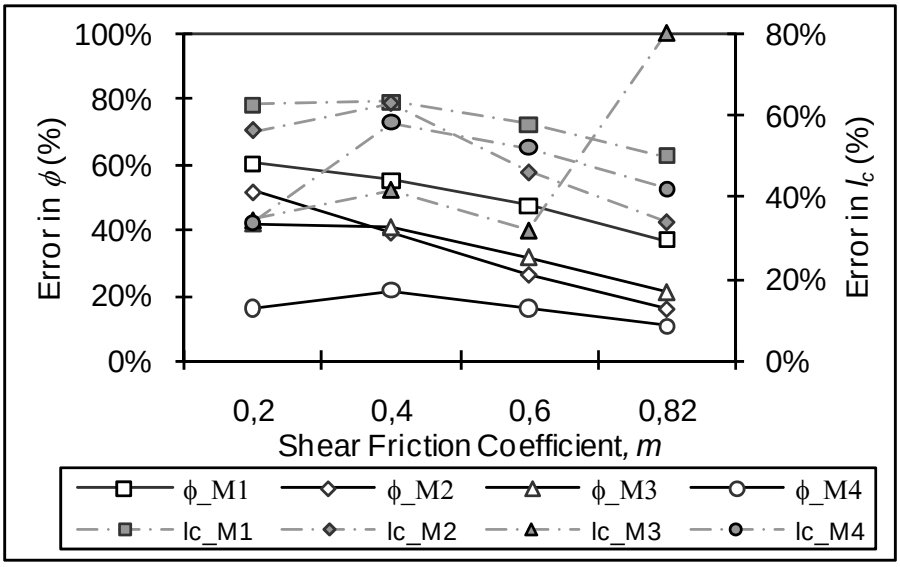

Figure 2.16. Percentage errors for shear angle and contact length using the constant shear model (V_c = 100 m/min, f = 0.1 mm/rev).

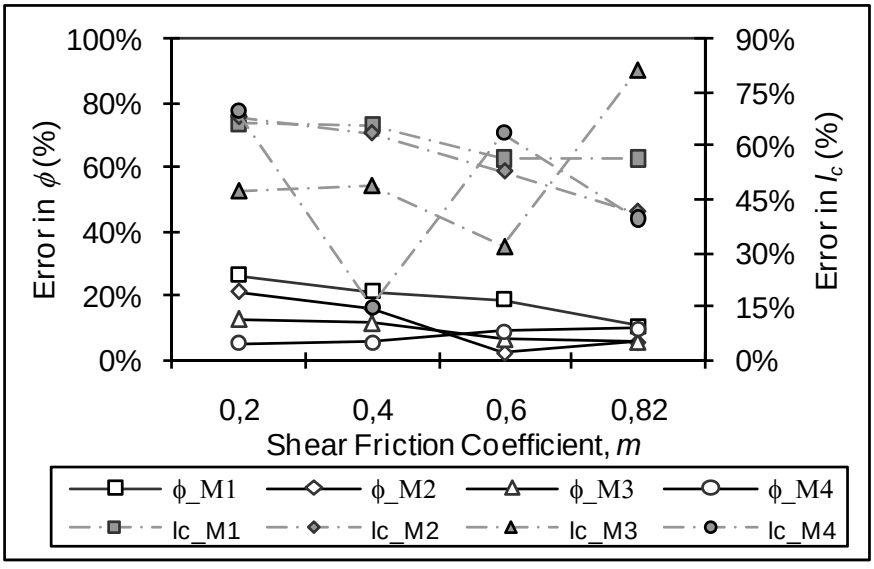

Figure 2.17. Percentage errors for shear angle and contact length using the constant shear model (V_c = 150 m/min, f = 0.1 mm/rev).

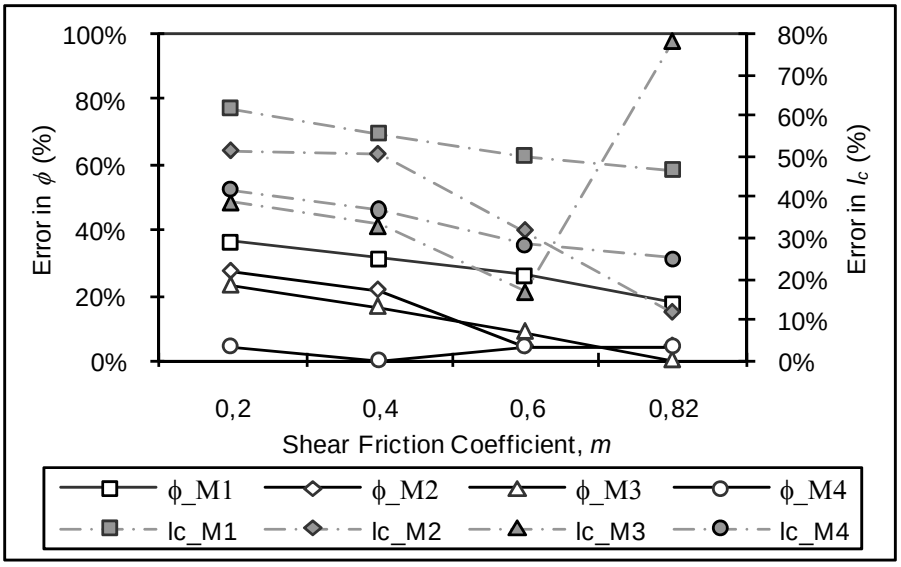

Figure 2.18. Percentage errors for shear angle and contact length using the constant shear model (V_c = 100 m/min, f = 0.15 mm/rev).

2.5.3.5 CUTTING CONTACT LENGTH AND SHEAR ANGLE PREDICTIONS USING THE COULOMB MODEL

In general, the situation does not change significantly utilizing Coulomb's friction model instead of the constant shear model (Figures 2.19, 2.20 and 2.21) as far as the prediction of the shear angle, ϕ, is concerned.

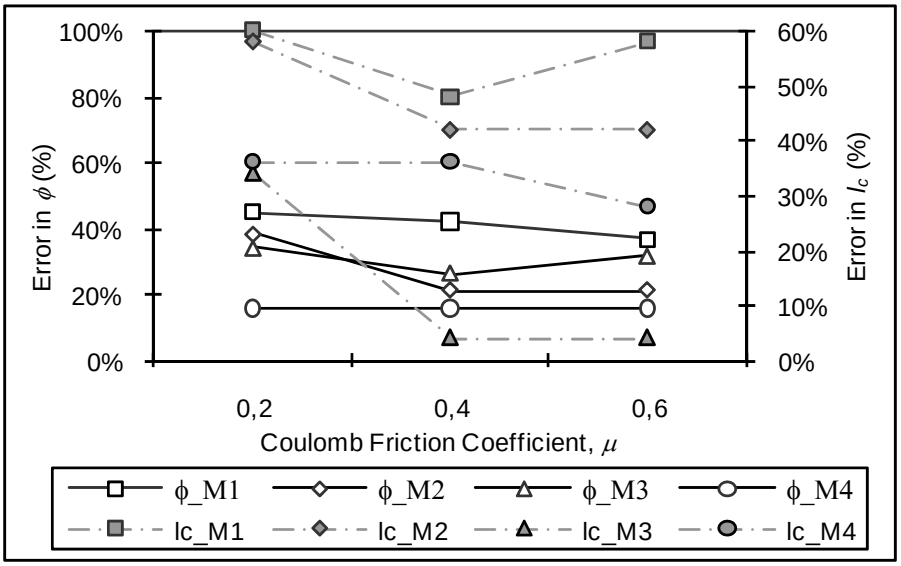

Figure 2.19. Percentage errors for shear angle and contact length using the constant coulomb model (V_c = 100 m/min, f = 0.1 mm/rev).

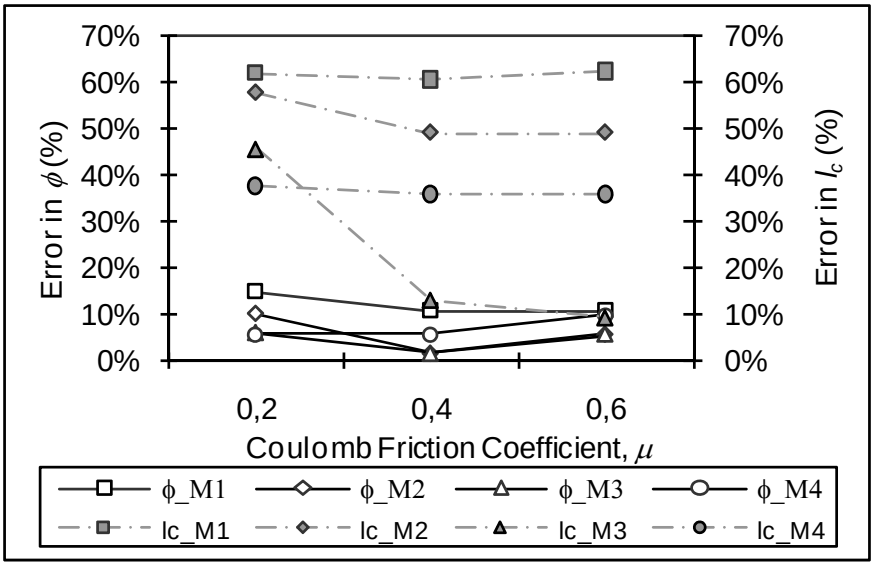

Figure 2.20. Percentage errors for shear angle and contact length using the constant coulomb model (V_c = 150 m/min, f = 0.1 mm/rev).

In fact, both M3 and M4 material models again show the best overall predictions at varying of both cutting speed and feed rate, even if for certain combinations of cutting conditions and friction coefficient, model M2 furnishes the best results as observed in Figures 2.20 and 2.21 for a friction factor μ = 0.4. Moreover, when the contact length, l_c, is investigated, the situation does not change considerably when utilizing Coulomb's friction model instead of the constant shear model (Figures 2.19, 2.20 and 2.21). In fact, M3 and M4 material models once more show the best predictions and, for both models, their relative errors decrease when larger friction coefficients are utilized.

2.5.3.6 CUTTING CONTACT LENGTH AND SHEAR ANGLE PREDICTIONS USING THE STICKING-SLIDING MODEL

The final investigation was carried out by analysing cutting contact length and shear angle predictions implementing the sticking-sliding friction law (Figures 2.22-2.24). Again, both M3 and M4 material models show, in general, the best predictions as far as the shear angle is concerned. In certain circumstances, model

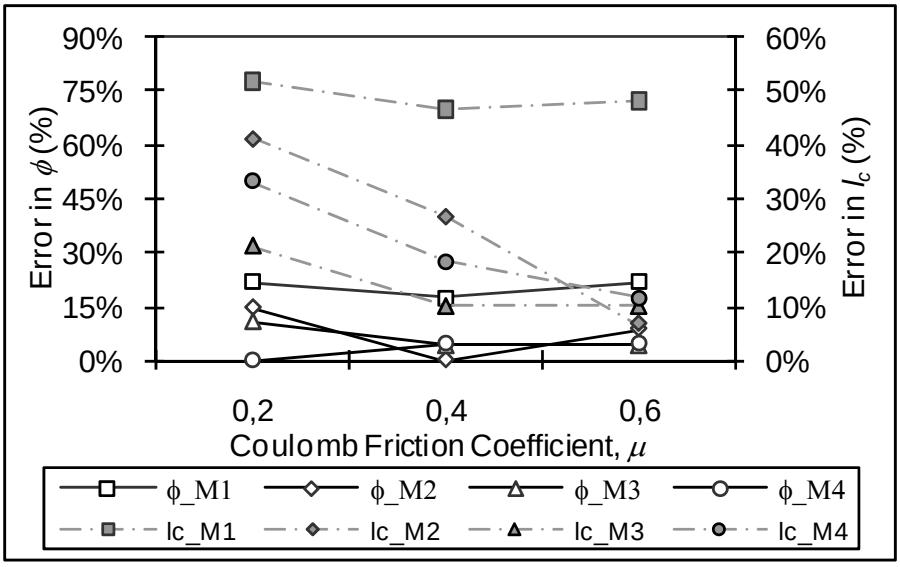

Figure 2.21. Percentage errors for shear angle and contact length using the constant coulomb model (V_c = 100 m/min, f = 0.15 mm/rev).

M2 furnishes the best result as observed in Figure 2.22 when the friction factor is equal to 0.4. In contrast, model M3, with the highest friction coefficient, gives suitable results when the contact length is taken into account. Therefore, when the sticking-sliding model is used, the best trade-off is given by model M3 since the prediction of the shear angle is correct while the contact length shows an error of about 20%.

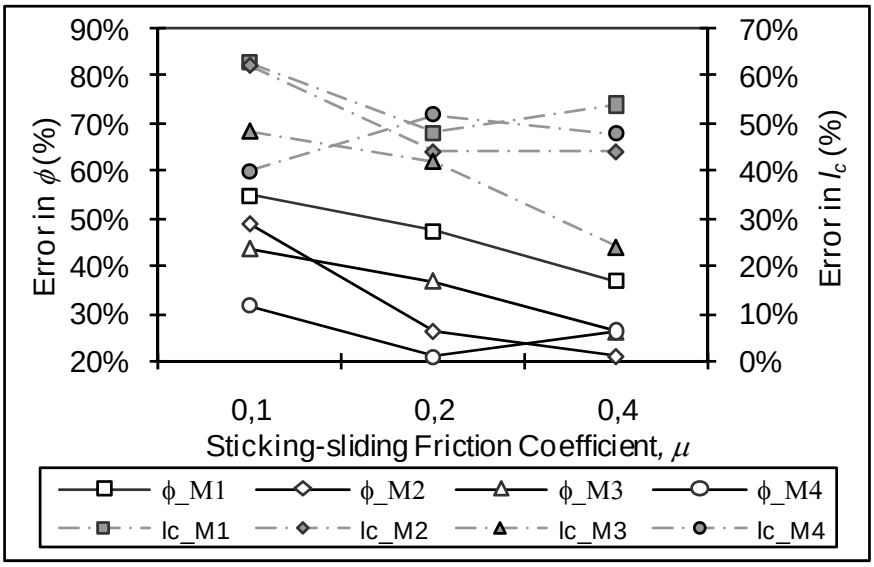

Figure 2.22. Percentage errors for shear angle and contact length using the sticking-sliding model (V_c = 100 m/min, f = 0.1 mm/rev).

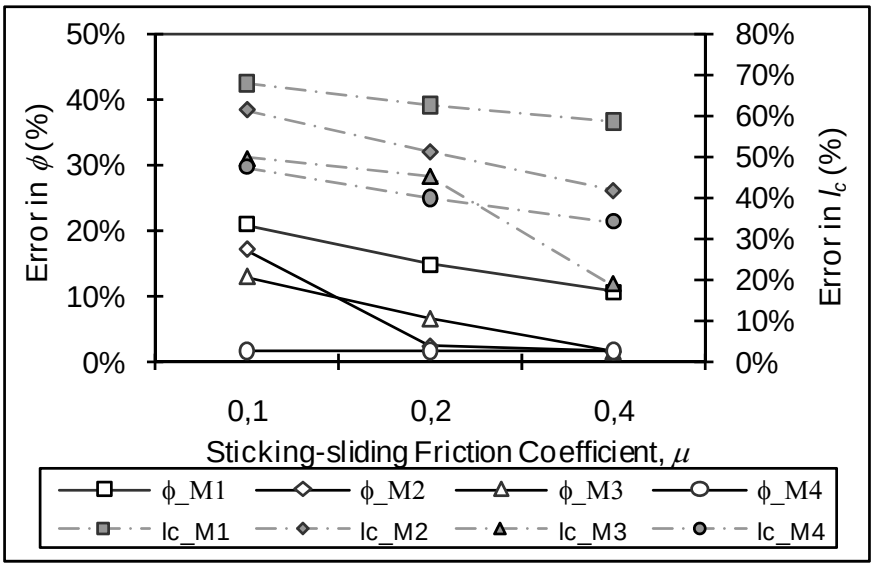

Figure 2.23. Percentage errors for shear angle and contact length using the sticking-sliding model (V_c = 150 m/min, f = 0.1 mm/rev).

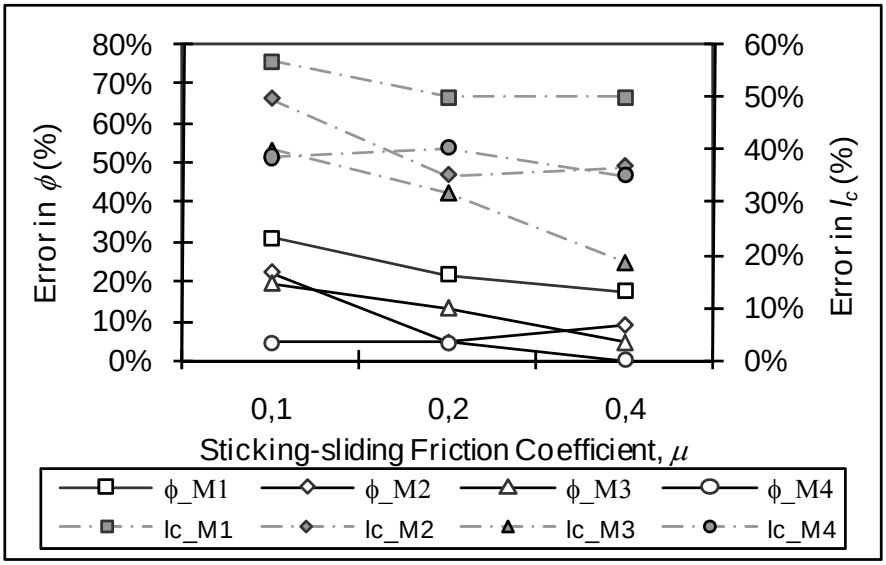

Figure 2.24. Percentage errors for shear angle and contact length using the sticking-sliding model (V_c = 100 m/min, f = 0.15 mm/rev).

2.5.4 RESULTS DISCUSSION

The data reported in all the previous figures confirm that, for any specific problem, there is a set of input data that ensures suitable outputs. In fact, it was noticed that material model M1 is generally the most appropriate to predict the principal cutting force, F_z, and, for a large number of variable combinations, the

thrust force, F_t, is also predicted with relatively low error. On the contrary, the corresponding errors relating to shear angle and contact length predictions are very high, sometime larger than 80%.

In contrast, a different trend is shown by material model M4, which provides relatively good predictions for both contact length and shear angle, but performs relatively poorly when the cutting force predictions are taken into account. Similar observations can be drawn for the other two utilized models.

Therefore, due to the relatively large amount of available data, the definition of a synthetic error index can help to make some general comparisons. This index was defined as an average value of the errors obtained in predicting each investigated variable with respect to the corresponding experimental values, for all the utilized cutting conditions, according to the following formula:

$$\bar{e}_{kp} = \frac{1}{n \cdot m} \sum_{i=1}^{n} \sum_{j=1}^{m} \left| \frac{x_{kp_{ij}} - \bar{x}_{kp_{ij}}}{\bar{x}_{kp_{ij}}} \cdot 100 \right| \tag{13}$$

where:

$\bar{e}_{kp}$ is the synthetic error index;

$x_{kp_{ij}}$ is vector of predicted variables by FE analysis;

$\bar{x}_{kp_{ij}}$ is vector of experimentally measured variables;

k is the number of material models (shown in Figure 2.6);
p is the number of friction conditions (reported in Table 2.17);
n is the number of experimentally investigated cases (Table 2.15);
m is the number of predicted variables (F_z, F_t, ϕ, l_c).

The obtained results are shown in Figure 3.25 which reports the synthetic error index, for all the friction conditions vs. the selected the material models. In the figure it is possible to observe a better behaviour of some material models, but also a strong dependence on the friction conditions. In particular, material model M3 in combination with Coulomb friction law, using a friction coefficient, μ, of 0.4 to 0.6 yielded the lowest synthetic error, while the material model M2 in

combination with constant shear friction model (m = 0.82) also gives comparably low synthetic error.

Though it can be noted that the synthetic error is never below 15%, and this may be considered as a relatively high value, however uncertainty in experimental measurements can sometimes be on the same order of magnitude. At the same time, the synthetic error can also be greater that 40% in the worst case, hence considerable scope exists for further improvements in simulation of machining processes. In fact, the main aim of this work is not simply to determine the best combination of material model and friction law, with appropriate friction coefficient, but to highlight the necessity to spend more efforts in advancing the capability of machining simulations.

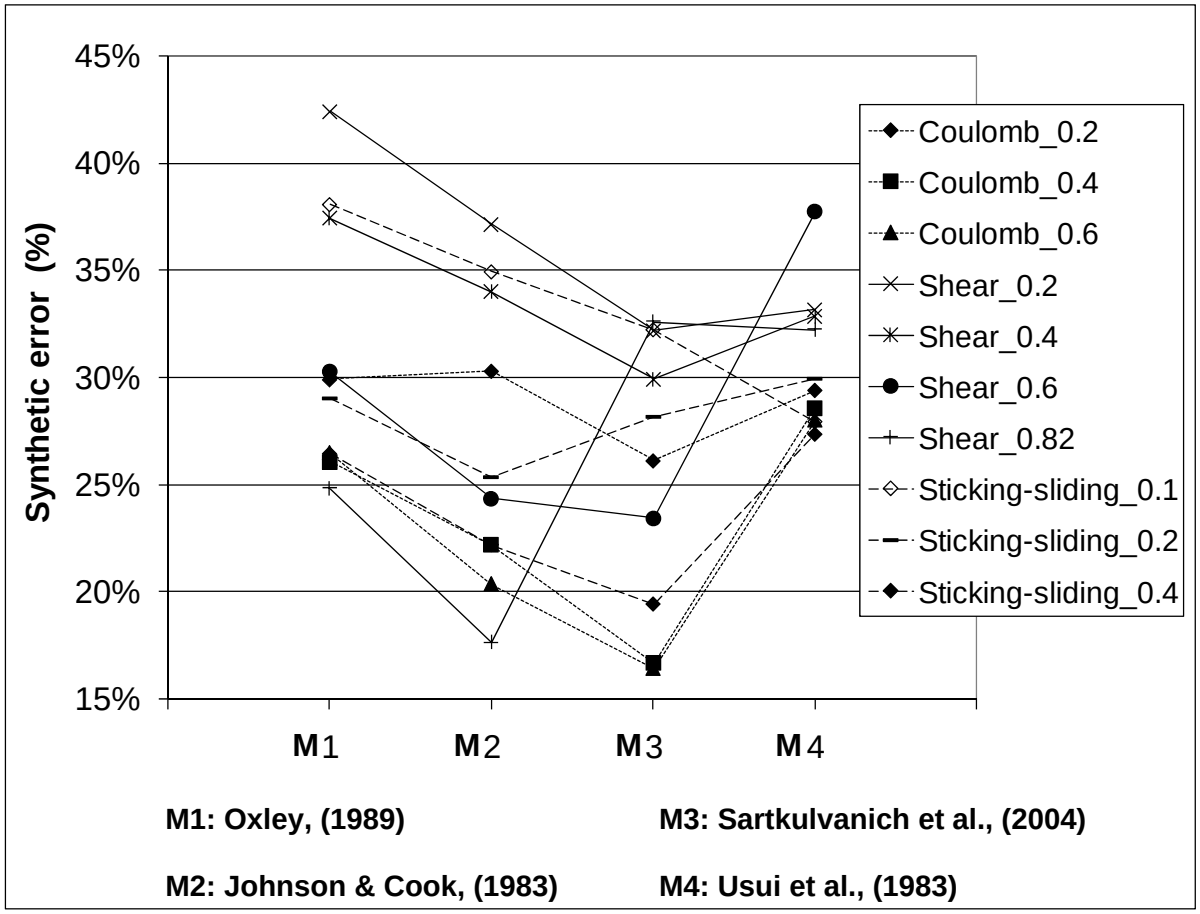

Figure 2.25. Synthetic error for different materials and friction models.

Concluding, the following major outcomes can be drawn from the investigation:

1. Due to the unique conditions arising in machining appropriate material models have to be developed. Differences up to 50% can be observed for the flow behaviour of the same material using different models;
2. The effectiveness of machining simulation varied with both material models and friction laws. For example:
   2.1 Material model M1 was found to be the most appropriate model for predicting the cutting forces under most cutting conditions and friction laws, however the corresponding errors relating to shear angle and contact length were very high;
   2.2 In contrast, a different trend was shown by material model M4, which provides relatively good predictions for both contact length and shear angle, but performs relatively poorly when the cutting force predictions are taken into account.
   2.3 Overall , the lowest synthetic error was obtained using material model M3 in combination with Coulomb friction law, using a friction coefficient of 0.4 - 0.6;
   2.4 Also, material model M2 in combination with constant shear friction model (m = 0.82) gave comparable synthetic error;
3. Though the synthetic error is never below 15%, however uncertainty in experimental measurements can sometimes be comparable or even higher;
4. The synthetic error can also be greater that 40% in the worst case, hence considerable scope exists for further improvements in simulation of machining processes.

2.6 CONCLUSIONS

Friction modelling is one the most critical aspects to be properly defined in FE simulation of machining.

The initial study focused only on one material and one process configuration, highlighted that, apart from small differences, the main mechanical results (i.e. forces, contact length and so on) are not much sensitive to friction model. On the

contrary, friction becomes probably the most relevant issue in thermal analysis since it determines the rake face heating.

Successively, some of the most common friction models were applied to different couples of tools and workpiece materials.

Also in these cases, a low sensitivity of the mechanical parameters on the friction model was observed. At the same time, the thermal aspects turned out to be once more, a point of weakness, since a generally applicable model is not yet available.

Finally, the results of a simulation study in which orthogonal cutting process of a plain-carbon steel was investigated at varying conditions of cutting speed and feed rate, were presented. Four different material constitutive equations and three different friction laws were implemented, and the numerical predictions were compared to the experimental evidences.

This analysis underlined that for any specific situation there is a specific set of input data that ensures suitable outputs.

The study, in fact, showed that some sets of material model laws, friction models and friction coefficients are able to well describe some variables, for instance the process forces, but the scenario changes when other variables are investigated.

Process complexity is so high and requires very accurate modelling of any aspect related to the process mechanics.

The complete examination of the results reported in this chapter allows to state that, despite the numerical investigation of machining began more than 15 years ago, some basic aspects have to be still improved.

Material modelling is one of them. A sufficiently robust approach to numerical simulation needs the development of more reliable models for material behaviour in the in-process conditions. Moreover, further efforts are necessary as far as the thermal aspects are regarded.

Both these topics, i.e. the material modelling and the heat transfer phenomena, were approached during this PhD thesis and they will be discussed in the following chapters.

CHAPTER 3

A NEW APPROACH TO MODEL HEAT TRANSFER PHENOMENA AT THE TOOL-CHIP INTERFACE

3.1 INTRODUCTION

How already mentioned, the use of numerical simulation for investigating machining processes by finite element simulations is remarkably increasing [20, 55, 72, 73] because of the simulation cost is lower than the experiments and the possibility to analyze local variables such pressures, strains, and temperatures is allowable. But, process simulation is very hard from a computational point of view, since it frequently requires remeshing phases and very small time steps, and often some heavy geometrical simplification have to be introduced.

In particular, usually a 2D simulation of orthogonal cutting process is taken into account and the total simulated time is very high low. In fact, only few milliseconds of the cutting operation can be simulated with an acceptable CPU time utilizing a 2D plane-strain analysis, at the current cutting speed of the order of some hundreds of meters per minute. This very low time introduces several problems if the focus of the analysis involves thermal issues, related to heat generation and diffusion into the tool [67, 74]. In fact, no steady-state conditions are reached during the numerical simulation.

Technical literature shows that it is relatively easy to predict some process variables such as the cutting and thrust force, the chip geometry, shear angle and

the contact length [60, 75-77]; on the contrary, the numerical prediction becomes absolutely poor when the temperatures on the rake face and inside the tool are investigated [67]. Different approaches were proposed to overcome this problem [62, 78-80]; for example, some researchers arbitrary modified the global heat transfer coefficient in order to accelerate the steady state achievement [50,81]. It's worth outlining that these techniques partially solve the problem but they are not able to properly take into account the physics of the process.

A new approach is proposed in this thesis. First of all, numerical simulation is based on a mixed updated Lagrangian – Eulerian approach: a preliminary mechanical analysis is carried out, utilizing the updated Lagrangian formulation; when steady conditions are reached (at least, as concerns mechanical variables, namely chip shape, contact length, cutting forces), the results are provided to the following coupled thermo-mechanical Eulerian analysis. Furthermore, heat transfer at the tool-chip interface was taken into account through the introduction of a global heat transfer (film) coefficient at the tool-chip interface, which was determined through an inverse approach utilizing a set of available experimental data. What is more, the dependence of such coefficient on physical variables (normal pressure and temperature on the rake face) was investigated, deriving an useful law on the basis of a regression procedure.

From a purely industrial point of view, it is easy to understand that a more consistent analysis of those phenomena related to the tool temperature, such as tool wear or material strength decreasing, is possible when a reliable methodology to estimate temperature distribution in the tool becomes available.

3.2 THE ROLE OF THE GLOBAL HEAT TRANSFER COEFFICIENT

Heat generated in machining is mainly due to the deformation work on the shear plane (primary shear zone) and to friction on the rake face along the chip-tool contact length (secondary shear zone). At the conventional cutting speeds, the largest part of heat is dissipated in the chip and only a low percentage flows towards the tool. The prediction of this quota represents a big challenge.

According to the above considerations, two aspects have to be carefully taken into account as far as heat flow prediction is concerned, namely the evaluation of the global heat transfer coefficient, *h*, at the chip-tool interface and the simulated cutting time. The coefficient is the physical variable which models the heat transfer at the tool-chip interface (Figure 3.1).

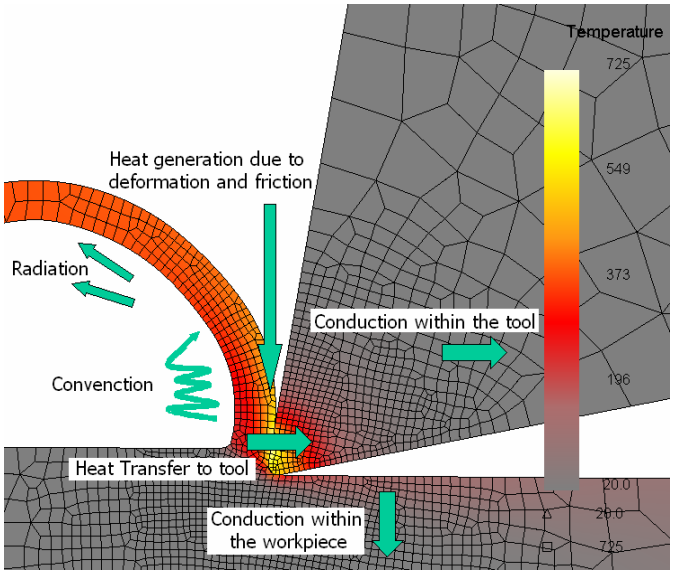

Figure 3.1. Heat propagation in the bodies and toward the environment.

In particular, in a cutting process the total heat flux Q is always given by the total amount of two quotas: the friction heat, Q_1, and the heat flux generated by the temperature difference at the tool-chip interface, Q_2 (Figure 3.2).

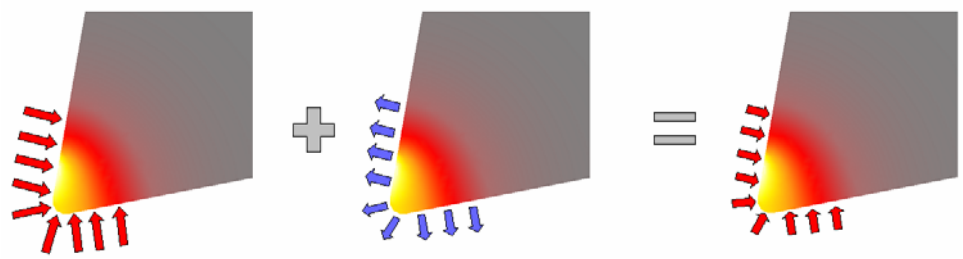

$$Q_1 = J \times \lambda \times \tau_f \times v_s \qquad Q_2 = h \times (T_W - T_T) \qquad Q = Q_1 + Q_2$$

Q_1 = Friction heat flux
λ = Heat partition factor
J = Energy conversion factor
τ_f = Shear stress at the interface
v_s = Sliding velocity

Q_2 = Contact heat flux
h = Global heat transfer coefficient at the interface
T_W = Workpiece contact temperature
T_T = Tool contact temperature

Q = Total heat flux applied to the contact elements at the tool-chip interfaces

Figure 3.2. Heat generation at the tool-chip interface.

Then, taking into account that the contact surface temperature of the chip, can be considered to be nearly independent of the global heat transfer coefficient, the physical property of h is considered only in the calculation of Q_2.

Because of the very short cutting time that can be effectively investigated using the Lagrangian formulation, some researchers [62,78] attempted to tune the global heat transfer coefficient with the aim to accelerate the convergence of finite element simulation towards steady state conditions. This time is not sufficient to permit that the generated heat in the primary shear zone arrives to the chip-tool interface and affects the temperature distribution in the tool. Therefore the calculated temperatures in the tool mainly depend on the heat generated by friction in the secondary shear zone and the global heat transfer coefficient works, more or less, as a *partitioning* coefficient which determines the heat amounts flowing into the chip and the tool respectively.

Despite the effectiveness of some temperature predictions reported in the literature, such method doesn't appear scientifically consistent, because it's not able to take into account the actual physical phenomenon.

The global heat transfer coefficient was experimentally measured in the past taking into account both the forming [82] and machining processes.

Childs et al. [83], in particular, in 1998 evaluated the coefficient taking into account the role of the coolant when machining a mild steel using a HSS tool, at different cutting speed, ranging from 33 to 61 m/min. They calculated the h value by the thermal equilibrium equations estimating the thermal distribution in the tool utilising a micro-hardness campaign of measurement.

In the proposed research, the study is carried out with the aim to build a ready to use system which is able to automatically calculate all the involved variables. In other words, in a first section of the study the h coefficient was estimated utilising a properly developed numerical-experimental procedure. Thus, the dependence of the coefficient on the average rake face normal pressure and temperature was formally established, as well as the dependence of the coefficient h on the cutting speed and the feed rate.

3.3 EXPERIMENTAL PROCEDURE

A set of experimental tests was firstly carried out in order to acquire the tool temperatures. The tests were carried out in orthogonal conditions. Disks with a thickness of 3 mm were cut using a tool with an edge width of 4mm. The turning operations were executed without any coolant at the tool-chip interface, utilizing a CNC lathe UTITA, with a power of 22 kW (Figure 3.3).

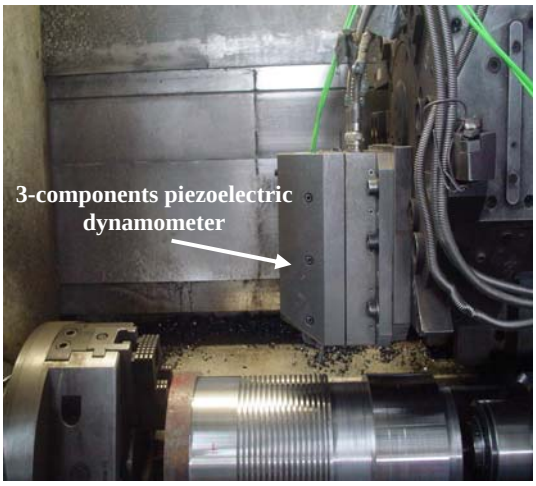

Figure 3.3. The experimental equipment.

The cutting tool was an uncoated carbide ISO P40, with a rake and a clearance angles of 10° and 11°, respectively. The workpiece material was an AISI1045 steel. The tests were executed at a cutting speed ranging from 50 to 150 m/min, and feed rate in the range 0.05 - 0.15 mm/rev. Cutting and thrust forces were measured by using a three-components piezoelectric dynamometer.

A Chromel/Alumel thermocouple (K type) with a diameter of 0.5 mm was properly forced into the tool cutting a hole by means of an Electrical Discharge Machine [79]. The thermocouple had a measure uncertainty of +/- 1.1°C or 0.4% and was placed in the tool at a distance "h_distance" from the rake face, according to the Figure 3.4.

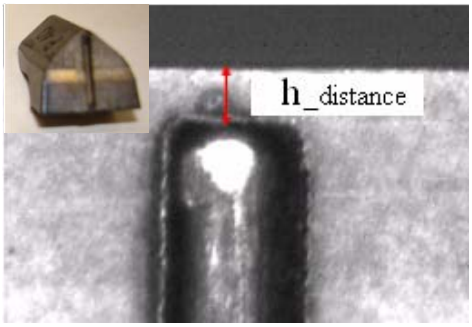

Figure 3.4. The ready-to-use equipped tool.

The experimental steady temperatures at varying of the cutting parameters are listed in Table 3.1, where T is the temperature revealed by the thermocouple and F_C the measured principal cutting force.

Table 3.1. The experimental results.

V_t(m/min)	a (mm/rev)	$h_{\_distance}$(mm)	T (°C)	F_c(N)
50	0.100	0.36	522	795
70	0.100	0.36	523	811
90	0.100	0.36	518	819
100	0.050	0.26	332	447
100	0.075	0.36	448	636
100	0.100	0.39	514	820
100	0.125	0.36	530	998
100	0.150	0.36	497	1170
110	0.100	0.39	509	819
130	0.100	0.36	494	810
150	0.100	0.36	474	794

3.4 PROCEDURE TO CALCULATE THE GLOBAL HEAT TRANSFER COEFFICIENT

As far as numerical simulations are concerned, the SFTC-Deform-2D code was utilized. The workpiece was initially meshed by means of 2500 iso-parametric quadrilateral elements while the tool, modelled as rigid, was meshed into 700 elements. A plane-strain updated-Lagrangian analysis was firstly carried out: no temperature effects were taken into account and the global heat transfer coefficient, h, was fixed equal to 0 kW/m^{2}K. The material behaviour was described using the Oxley model [56]. The scheme of both the thermal and the mechanical initial boundary conditions is shown in Figure 3.5.

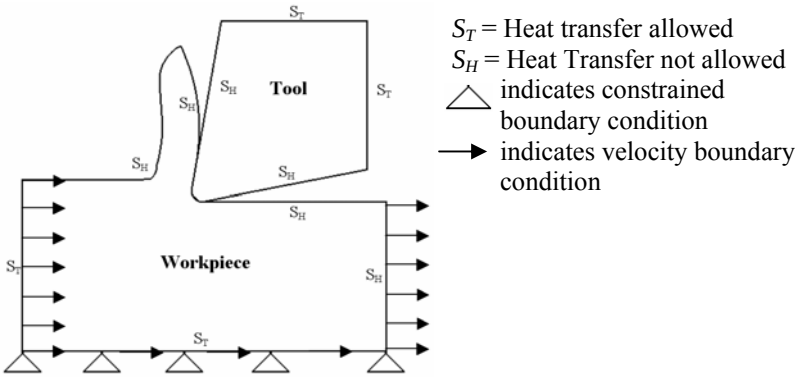

Figure 3.5. Scheme of initial boundary conditions.

As concerns friction, a simple model based on the constant shear hypothesis was implemented, setting m=0.82 in the friction law described by the equation (1):

$$\tau = m\tau_0 \tag{1}$$

being τ the shear stress and τ_0 the flow shear stress obtained as:

$$\tau_0 = \frac{\sigma_0}{\sqrt{3}} \tag{2}$$

When steady-state conditions were reached (as concerns cutting forces, chip thickness, shear angle, chip-tool contact length), a coupled thermo-mechanical Eulerian analysis was started based on the outputs of the previous one (geometry, velocities, forces and so on). In other words, the Lagrangian incremental simulation was transformed into a steady-state machining simulation, in the Eulerian domain.

As mentioned, the latter was a coupled thermo-mechanical analysis, where the global heat transfer coefficient, *h*, was determined using the following iterative procedure:

1. set *h* equal to 100 kW/m^{2}K; [h:=100]
2. start the steady-state simulation;
3. calculate the predicted average steady–state temperature in the tool area corresponding to the thermocouple position (see Figure 3.6);

4. compute the error between the predicted and the experimental temperature; [e:= T_{NUM} - T_{EXP}]

4.1. if the error is lower than an acceptable threshold (minimum error lower than 0.5%) then stop;

4.2. else, tune *h* according to the obtained error and go back to step 2. [h:= h + k*e, where k is a gain coefficient]

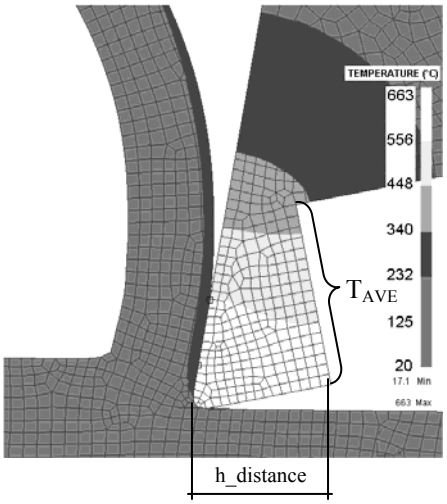

Figure 3.6. FEM model.

Some tests have been carried out in order to verify the sensitivity of the calculated *h* values depending on the thermocouple uncertainty. In particular, the *h* variation was always less than 1%.

3.5 RESULTS ANALYSIS

The described approach was applied to the whole set of experimental tests reported in Table 3.1. The calculated global heat transfer coefficients are reported in Table 3.2; in the same Table the predicted cutting force, the average temperature and the average pressure on the rake face of the tool are reported as well, both calculated along the predicted contact length.

Table 3.2. Predicted forces, average temperature on the rake face, average normal pressures on the rake face and global heat transfer coefficients.

V_t(m/min)	a (mm/rev)	F_c(N)	p_{rake} (MPa)	T_{rake} (°C)	h (kW/m^{2}K)
50	0.1	850	982	638	4
70	0.1	830	1013	705	14
90	0.1	814	1040	774	54
100	0.05	420	1087	506	186
100	0.075	595	1070	654	106
100	0.1	773	1053	808	93
100	0.125	941	1036	968	113
100	0.15	1112	1020	1135	203
110	0.1	802	1065	843	128
130	0.1	794	1086	913	213
150	0.1	790	1104	984	320

The above data were analyzed in order to assess the dependence of the global heat transfer coefficient on the average normal pressure on the rake face and on the average temperature on the rake face, along the contact length. A consistent model, characterized by a very high correlation index, equal to 0.99, was found out:

$$h = 17529 - 34.752 \cdot p - 1.019 \cdot T + 0.01756 \cdot p^2 + 0.000783 \cdot T^2 \ \text{[kW/m}^2\text{K]} \qquad (3)$$

being p and T the average normal pressure on the rake face in MPa and the average temperature along the contact length in °C, respectively.

The coefficient h can also be related to the cutting parameters (cutting speed V_C, and feed rate f), obtaining this expression:

$$h = 442 - 2.36 \cdot V_c - 7950 \cdot f + 0.0276 \cdot V_c^{\,2} + 406000 \cdot f^2 \ \text{[kW/m}^2\text{K]} \qquad (4)$$

For sake of completeness, the h trend versus the process parameters was investigated as well. Figure 3.7 shows that the global heat transfer coefficient increases at increasing the cutting speed while presents a more complex dependence at increasing the feed rate as reported in Figure 3.8.

Fundamental studies on thermal exchange between two in-contact bodies demonstrated that the global heat transfer coefficient increases if both the pressure and the temperature at the interface increase.

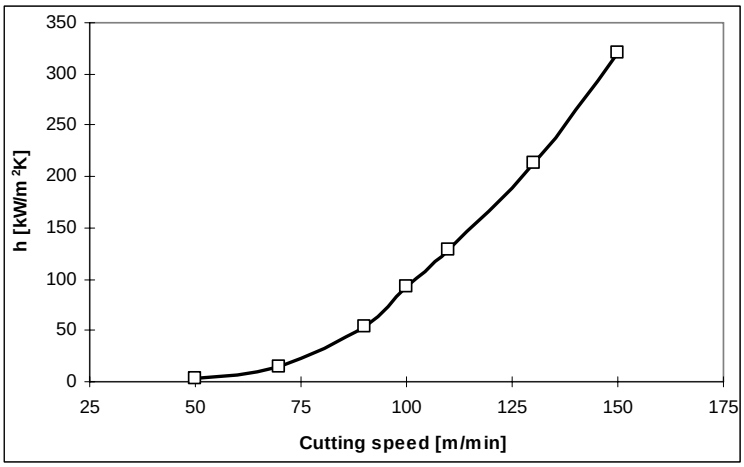

Figure 3.7. Dependence of *h* on cutting speed for a feed of 0.1 mm/rev.

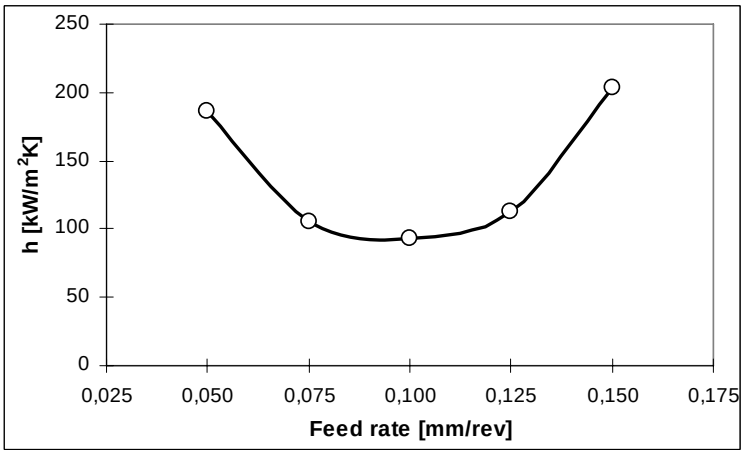

Figure 3.8. Dependence of h on feed rate for a cutting speed of 100 m/min.

Figures 3.9 and 3.10 show that, at increasing cutting speed, both the average temperature and pressure on the rake face increase (Figure 3.9). For this reason the continuous increasing of *h* vs. cutting speed is obtained (Figure 3.7).

On the contrary, at increasing the feed rate, temperature increases while the contact pressure decreases (Figure 3.10). Then, since the *h* value is dependent on both the above mentioned variables, the slope shown in Figure 3.8 is obtained.

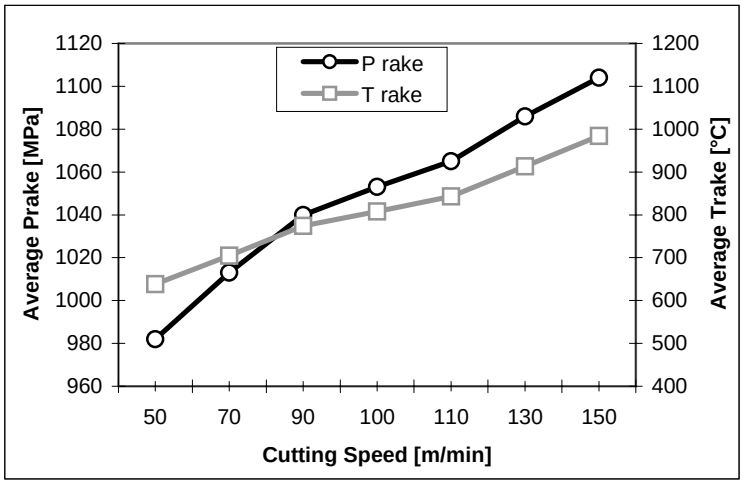

Figure 3.9. Dependence of average temperature and pressure on the rake face on cutting speed.

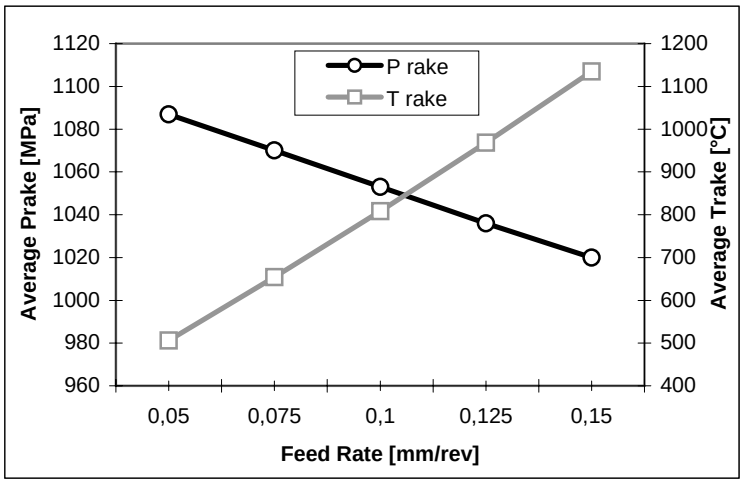

Figure 3.10. Dependence of average temperature and pressure on the rake face on feed rate.

3.6 CASE STUDY: 3D FINITE ELEMENT ANALYSIS OF TOOL WEAR

Tool wear is of great significance in manufacturing because it affects the quality of the components, tool life and machining costs. For this reason a relevant number of papers on tool wear can be recognized in literature.

Most of them are mainly based on empirical methods [84-87] or experimental studies [88-91], while only few regard the simulation of tool wear [62, 92, 93]. Moreover, until now the attention was mainly focused on 2D simulation in

orthogonal cutting conditions, since 3D models are very time consuming and are not reliable in terms of prediction accuracy. Nowadays, the increase of hardware and software efficiency makes 3D models effective to simulate actual machining processes. In particular, remeshing algorithms permit to manage complex geometries with a suitable accuracy despite of the still high calculation time.

This study was developed according to the described strategy. In fact, the study aims to scale-up the knowledge acquired with 2D models to 3D ones in order to obtain results which are closer to the industrial needs. In particular, a simple turning process of an AISI 1045 specimen using an uncoated WC tool was investigated. Flank and crater wear evolution was predicted utilizing a diffusion wear model implemented into an Arbitrarian Lagrangian Eulerian (ALE) numerical formulation. The model was firstly calibrated through 2D simulations and orthogonal experimental tests; then a 3D analysis, provided with a new 3D updating procedure for the dynamic prediction of the tool wear was carried out. Finally, a series of three dimensional experimental tests was carried out in order to validate the simulation strategy.

3.6.1 THE PROPOSED TOOL WEAR MODEL

According to the technical literature, several wear mechanisms can be defined, namely abrasion (related to thermo - mechanical action), adhesion (related to micro – welding and Built – Up Edge formation and removal), diffusion (chemical alteration due to atomic migration at high temperature), and fatigue. The above phenomena are generally present in combination, even if one or few of them are dominant (depending on the cutting parameters and tool-workpiece combination). For this reason, it is very difficult to define a general effective criterion for tool wear, as the proposed models are focused on some of the main wear mechanisms only.

Among all the proposed models, the Takeyama and Murata one [86] is able to properly take into account the abrasion and diffusion wear effects. As far as the mechanical abrasion is concerned, it is directly proportional to the cutting distance

and closely related to shape, hardness and distribution of the abrasive particles. Whereas the diffusion term is a physico-chemical contribution associated with the temperature.

Although the wear model depends upon the cutting conditions, the diffusive term is the predominant one for uncoated tools under standard conditions. This was confirmed by Mathew [94], who observed that if the temperature exceeds 700-800 °C , the abrasive term in Takeyama and Murata wear model can be neglected.

Moreover, the abrasion term can be neglected also according to the high hardness of tungsten carbide [20], which offers a strong abrasion resistance if the work material is not so hard. Finally Takeyama and Murata [86] demonstrated that abrasion rate of a tool is almost independent on temperature, if the latter is lower than the critical temperature of the tool material. Therefore at high temperatures the diffusion mechanisms prevails and this mechanism only was considered in the present study, utilizing the modified Takeyama and Murata model:

$$\frac{\partial w}{\partial t} = D \cdot \exp\left(-\frac{E}{R \cdot T}\right) \tag{5}$$

being D a material constant, E the activation energy (75,35 kJ/mol), R (8,314 kJ/mol K) the gas constant and T the local temperature, measured in K. Thus, the calibration of parameter D, as a function of both cutting time and temperature, assumes dramatic importance.

Moreover, the effectiveness of the model strongly depends on the prediction of temperature distribution in the tool [95]. The above considerations highlight two critical points: the evaluation of the parameter D and the effectiveness of temperature prediction.

As far as the latter is concerned the ALE approach previously presented was used. Temperature predictions were obtained by means of the Eulerian step of the analysis, assuming the global heat transfer coefficient at the tool-chip interface, h, as a function of both the cutting speed ,V_C, and the feed rate, f.

On the other hand, in order to calibrate the parameter D in (1) some 2D simulations and orthogonal cutting tests were carried out.

In particular, two preliminary tests were performed utilizing two cutting speeds (100m/min and 150m/min) and a fixed feed rate (0.1mm/rev). Disks with a thickness of 3 mm were cut using uncoated ISO P40 tool with an edge width of 4 mm, rake angle γ=10° and clearance angle α=11°.

The operations were executed in dry conditions utilizing a CNC lathe. Tool wear was measured using an optical microscope (50X), while tool temperature was revealed utilising an embedded Chromel/Alumel thermocouple (K type) with a diameter of 0.5 mm and an uncertainty of +/- 0.4%. The distance between the rake face and the thermocouple was fixed to 0.73mm for V_C=100m/min and 0.5mm for V_C=150m/min (Figure 3.11).

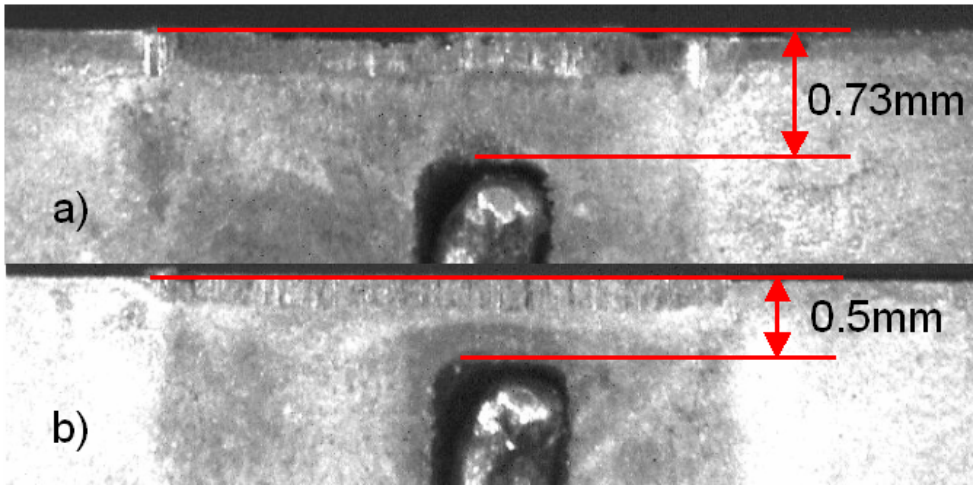

Figure 3.11. The equipped tools: (a) test: V_C=100m/min – f=0.1mm/rev; (b) test: V_C=150m/min – f=0.1mm/rev.

Table 3.3 reports the measured flank wear data and the temperatures into the tool for different cutting times. The table also reports the temperature values calculated through the ALE simulations. The relative errors ranged within -10 and 1%.

Table 3.3 also shows that the wear rate can be considered independent on the cutting time (after few minutes), while it is related to the process parameters and, therefore, to the temperature.

Table 3.3. Experimental flank wear (V_B), measured and predicted temperatures.

Test	t min	V_B μm	$\Delta V_B/\Delta t$ μm/min	T_{EXP} °C	T_{NUM} °C
V_C=100m/min f=0.1mm/rev h=93kW/m^2°C	0.6	20	33.3	388	360
	2.2	40	12.5	402	387
	8.8	97	8.6	399	364
	15.5	151	8.1	407	395
	32.3	284	7.9	426	416
V_C=150m/min f=0.1mm/rev h=320kW/m^2°C	1	65	35	426	411
	2	95	30	426	386
	3	120	25	426	409
	4	140	20	440	424
	5	161	21	459	418
	6	180	19	497	465

Therefore, a new plan of 2D orthogonal experiments was designed in order to further investigate the correlation between the flank wear evolution and the machining process parameters. Table 3.4 reports the utilized cutting conditions and the measured average flank wear data.

Table 3.4. Measured flank wear after 5 min cutting time.

f [mm/rev]	Vc [m/min]		
	100	150	200
0.10	0.071 mm	0.161 mm	0.208 mm
0.15	0.173 mm	0.210 mm	0.278 mm
0.20	0.195 mm	0.232 mm	0.330 mm

The use of flank wear measurements only is based on the observations made by Kitagawa [96], who highlighted that both flank and crater wear follow the same mechanism.

All the tests reported in Table 3.4 were numerically simulated, utilizing the ALE approach and the Takeyama and Murata wear model. An inverse approach was carried out to calculate the optimal D value for each test condition, allowing the best match between numerical wear predictions and experimental data. In this way it was possible to assess that D depends on tool temperature according to a third order polynomial law.

Figure 3.12 shows the obtained equation, where T is the local temperature, in K.

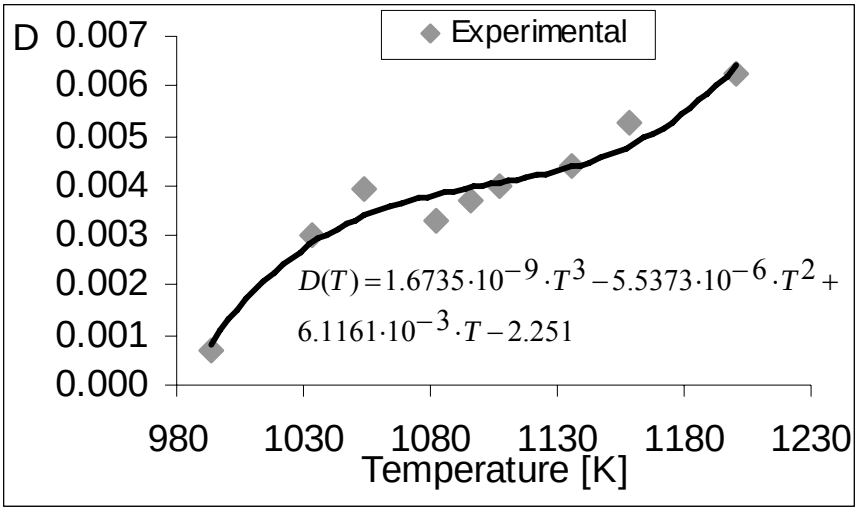

Figure 3.12. Evolution of parameter D vs. temperature.

SFTC Deform 2D® numerical code was utilised for the plane strain simulations. The Oxley's law was implemented to describe material flow as a function of strain, strain rate and temperature according to the FE code database.

As far as friction is regarded, a simple constant shear model was implemented and the friction factor, m, was set equal to 0.82.

3.6.2 3D EXPERIMENTAL TESTS

As already announced, this study was aimed to the 3D numerical prediction of tool wear using the knowledge acquired in 2D studies. Thus, in order to validate 3D predictions for both flank and crater wear, a series of experiments was carried out in 3D turning.

Cylindrical bars with a diameter of 100 mm were cut using an uncoated ISO P40 tool with tool nose radius of 0.8mm, rake angle γ=0°, clearance angle α=6° and inclination angle λ=7°.

Furthermore, the tool was positioned into the tool holder in order to obtain the angles χ and χ' of 90° and 30°, respectively, as illustrated in Figure 3.13.

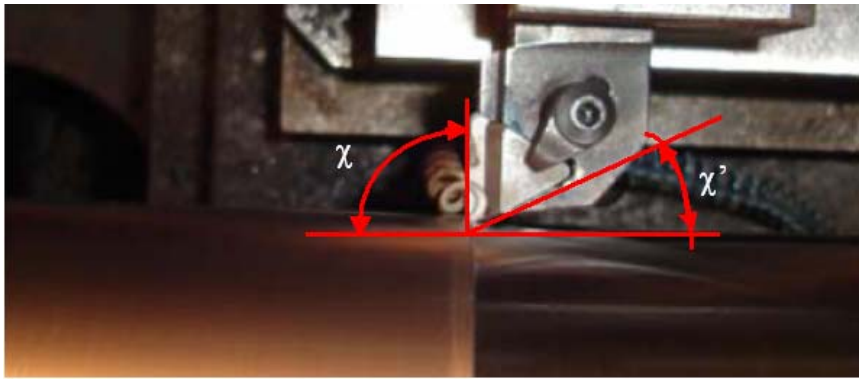

Figure 3.13. The experimental set-up for 3D tests.

Several levels were selected for each parameter, namely 150, 160 and 190 m/min (cutting speed), 0.17, 0.18 and 0.25 mm/rev (feed rate), while the depth of cut was fixed to 1.5mm. The operations were conducted in dry conditions and both flank and crater wear were measured at different cutting times, using an optical microscope (50X) equipped with a motorized faceplate. Table 3.5 reports tool wear data for the 3D experiments.

Table 3.5. Experimental tool wear in 3D cutting.

V_C m/min	f mm/rev	Time min	V_B mm	K_M mm	K_T mm
150	0.17	1	0.134	0.389	0.027
		2	0.148	0.476	0.038
		4	0.184	0.554	0.074
		6	0.199	0.497	0.095
160	0.25	1	0.122	0.548	0.02
		2	0.143	0.558	0.048
		4	0.194	0.686	0.099
		6	0.247	0.693	0.110
190	0.18	1	0.162	0.475	0.042
		2	0.176	0.467	0.076
		4	0.212	0.576	0.092
		6	0.239	0.656	0.132

3.6.3 3D NUMERICAL MODELLING

The 3D ALE simulation was carried out using SFTC Deform 3D. Material data were the same as above, while the heat transfer coefficient, h, was calculated using (2).

Figure 3.14 shows the 3D model. The workpiece is a rigid-plastic object, initially meshed with 45,000 elements, and the tool is a rigid object meshed with more than 100,000 elements.

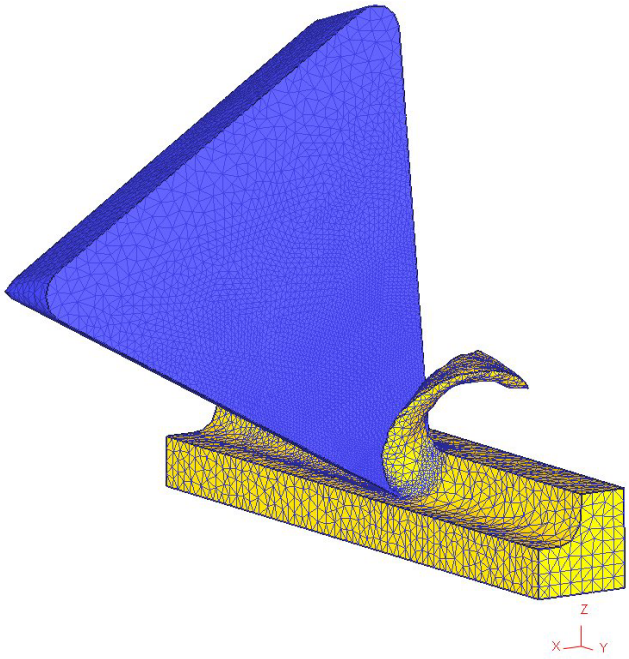

Figure 3.14. The 3D model.

The utilized numerical procedure can be summarized as follows: the first step is a coupled thermo-mechanical analysis, using an updated Lagrangian formulation, to reach mechanical steady state conditions. Then, the Eulerian step is carried out to determine temperature distribution.

Finally, the wear subroutine is called, tool wear is calculated and the geometry of the worn tool is updated. For each tool node the wear rate is calculated according to (1), afterwards the direction of the node movement is identified and, in the last step of the subroutine, the tool mesh and the tool geometry are updated.

The procedure is carried out subdividing the total cutting time in several steps and repeating the procedure until the total cutting time is reached. It is important to underline that the geometry updating is carried out starting from the tool worn geometry of the previous step and changing the node positions on the basis of the

new wear rate values. Indeed, the first step of the wear loop starts from the new flat tool geometry.

Figure 3.15 shows the updated tool geometry after 1, 2, 4 and 6 min cutting time.

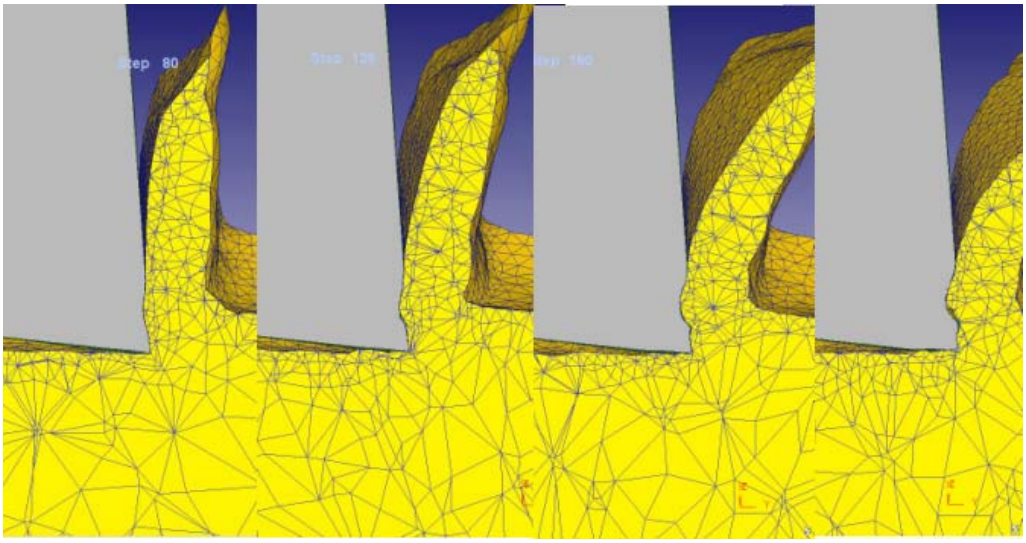

Figure 3.15. Development of tool wear after 1, 2, 4 and 6 min cutting time (V_C =160m/min, f=0.25mm/rev).

3.6.4 RESULTS AND DISCUSSION

Once the 3D simulative strategy for tool geometry upgrading was implemented, the attention was focused on flank and crater wear prediction at the varying of cutting velocity and feed rate for different cutting times.

Figure 3.16 shows the trend of simulated and experimental flank wear for the analyzed cases at different cutting times. All the experiments were repeated three times showing an uncertainty of +/- 6-10% (95% confidence interval). Observing these results it is evident the good agreement (the average error is about 6%).

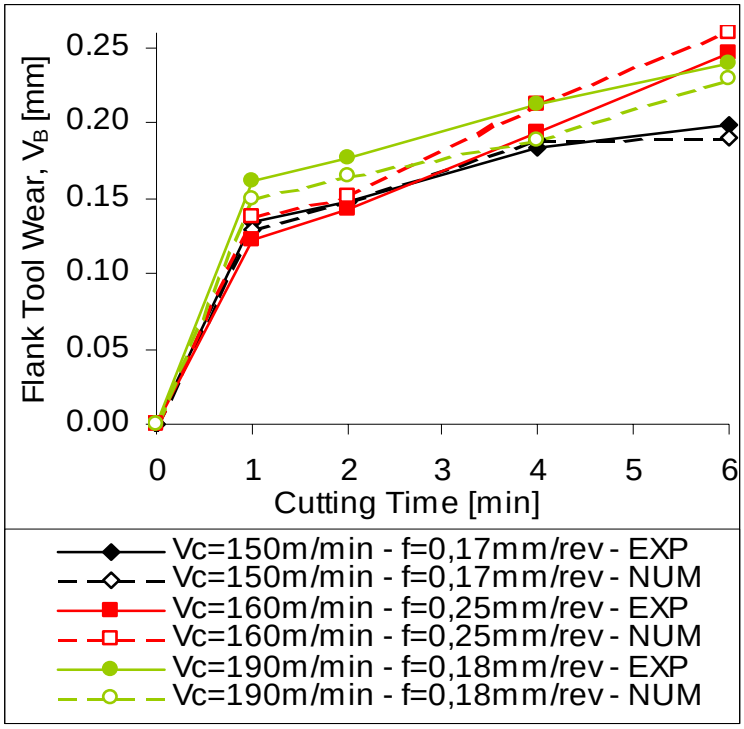

Figure 3.16. Simulated and experimental flank wear trends as function of cutting time.

Good results were found for crater wear simulation too. Figure 3.17 shows the experimental and simulated crater wear images super imposed for the case of V_C=160m/min and f=0.25mm/rev after a cutting time of 1 and 6 minutes. The overall good matching is evident.

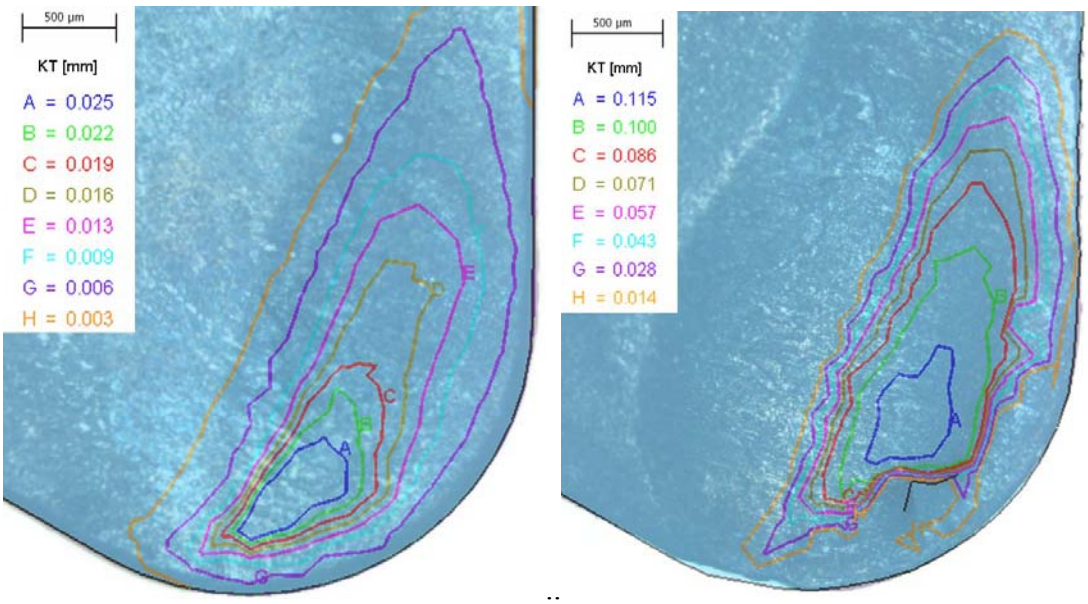

Figure 3.17. Experimental and simulated crater wear after 1 and 6 minutes (V_C =160m/min, f=0.25mm/rev).

Figure 3.18 shows the trend of simulated and experimental crater wear (K_T/K_M) for the analyzed cases at different cutting times. Also for the crater wear parameters, the experiments were repeated three times showing a combined uncertainty of +/- 8-13% with a confidence interval of 95%.

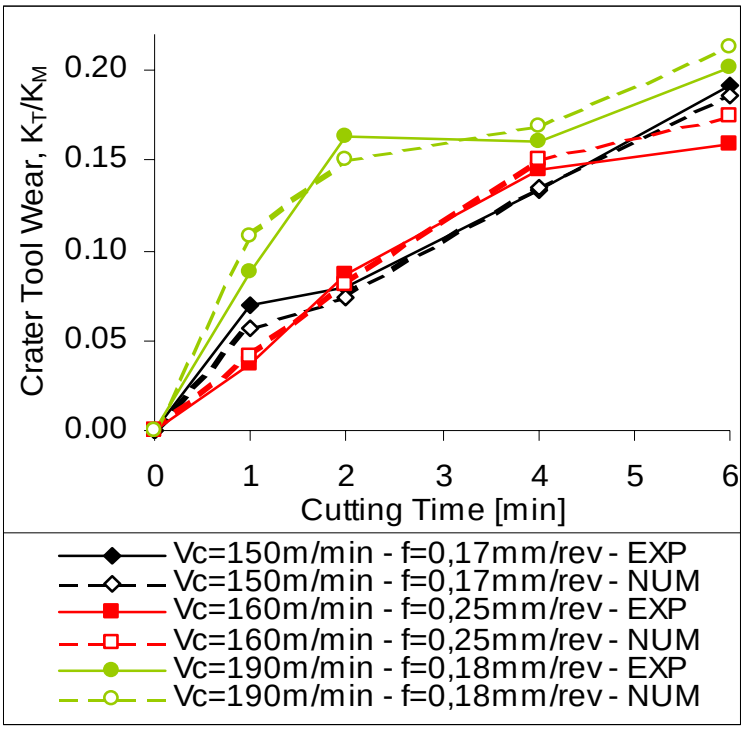

Figure 3.18. Simulated and experimental crater wear as function of cutting time.

3.7 CONCLUSIONS

Many efforts of researchers involved in cutting simulation are oriented to the full understanding of the thermal phenomena involved in the process.

In fact, in FE simulation of machining operations thermal exchange phenomena at the chip-tool interface are usually modelled as a black-box since it is impossible to reach the thermal steady state conditions by a simple Lagrangian simulation.

In this chapter a new physically-consistent model was proposed taking into account two relevant interface process variables such as contact pressure and

temperature. In particular the proposed law of the global heat transfer coefficient was developed fitting experimental-numerical data.

In this way it is possible to implement a proper function of *h* directly in the FE numerical code so to calculate the real amount of heat that flows between chip and tool as the contact pressure and temperature are varying during the cutting process.

As far as the case study is concerned, it can be stated that the implemented wear model furnished quite good results in terms of maximum flank wear and crater depth and position (K_T and K_M). In turn, larger errors were found for the crater area prediction: the simulated worn area is always lower than the experimental one as shown in Figure 3.17. This should be due to the fact that the implemented wear model takes into account the diffusive wear mechanism only, which is activated for a tool rake face temperature higher than 800°C. Therefore the tool areas at temperatures lower than this threshold are not considered worn in the simulation.

It is worth outlining that the developed model permits a quite satisfactory wear prediction for 3D cutting conditions and it represents a useful approach also for industrial needs.

CHAPTER 4

DEFINITION OF MATERIAL MODELS THROUGH MACHINING TESTS

4.1 INTRODUCTION

In order to obtain reliable results from numerical simulations, it is necessary to determine, as input, the properties of the workpiece and tool materials, as well as the characteristics of the tool/chip interface. These input data include physical and thermal data, friction and heat transfer, and most importantly, the flow stress of the workpiece material under high strain, strain rate and temperature conditions that exist during the process.

Actually, material behaviour modelling is usually regarded as a known issue since several laws are easily recognizable in literature [52, 56, 69, 71], almost for the most diffused materials. As observed in the previous chapters, these existing laws can be successfully utilized in the numerical simulation of cutting process, but only if the entire system is adequately set, in terms of friction model, friction coefficient, global heat transfer coefficient, and so on. In addition, they present a restricted validity, limited to reduced ranges of strain rate and temperature. For this reason, they are not applicable in many typical machining conditions, for instance when high cutting speeds are taken into account. Moreover, comparing the different laws, it is possible to recognize also relevant discrepancies that suggest to investigate more deeply in that direction. For example, it can be noted

that different chip shapes are observed when four common material laws are used in the numerical simulation of an orthogonal cutting process (Figure 4.1).

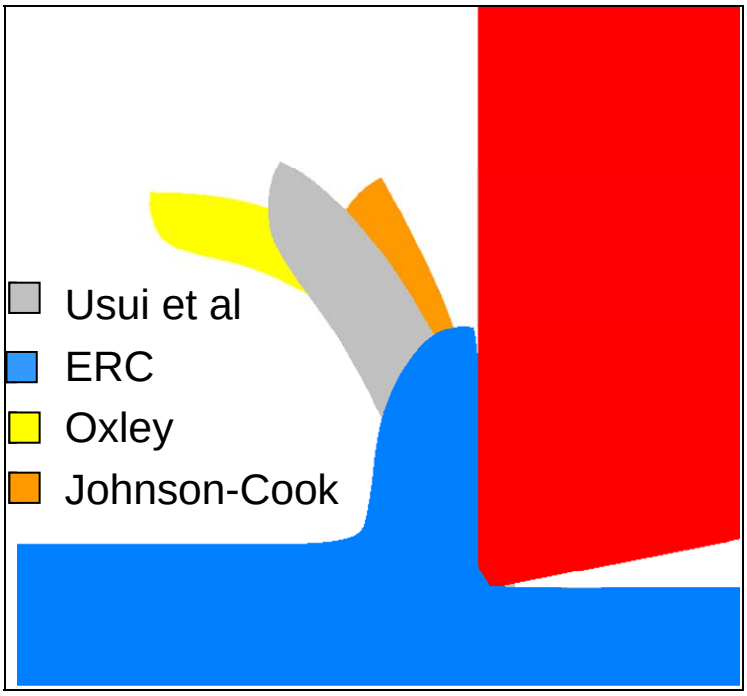

Figure 4.1. Simulated chip in orthogonal cutting of AISI 1045 steel (V=150 m/min, f=0.1 mm/rev; Friction model: constant shear, m=0.82).

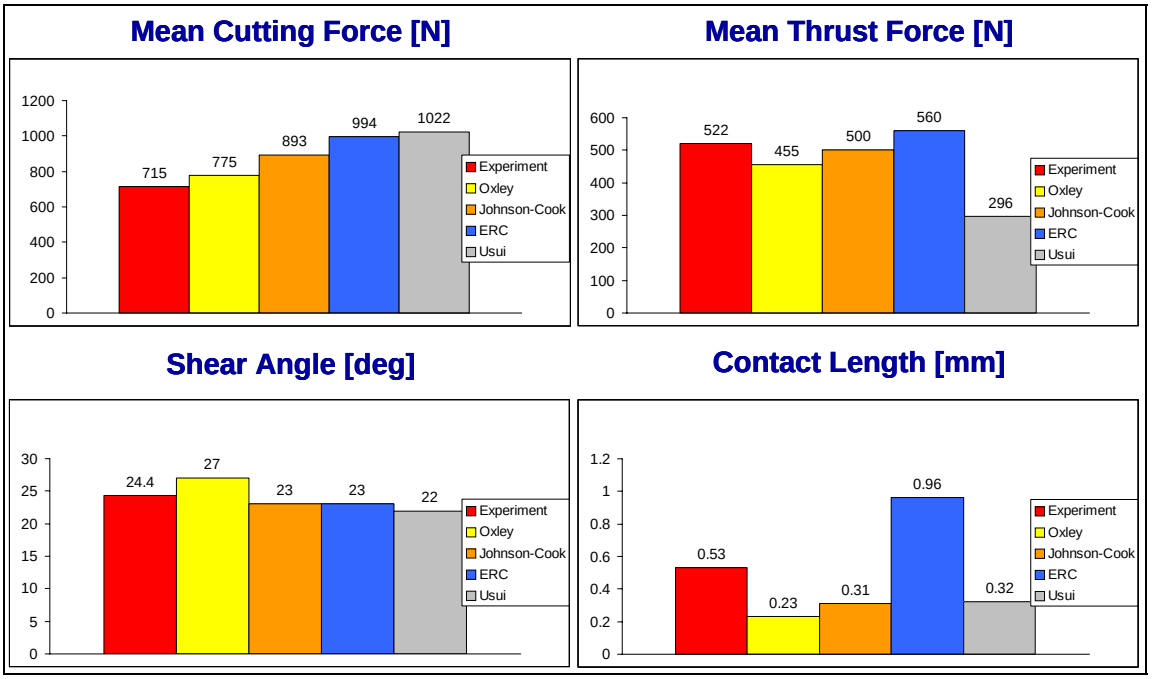

Figure 4.2. Predicted forces, shear angle and contact length in orthogonal cutting of AISI 1045 steel (V=150 m/min, f=0.1 mm/rev; Friction model: constant shear, m=0.82).

Other important differences can be observed in terms of predicted forces, shear angle and contact length (Figure 4.2), as well as concerning temperature distributions and maximum temperature (Figure 4.3).

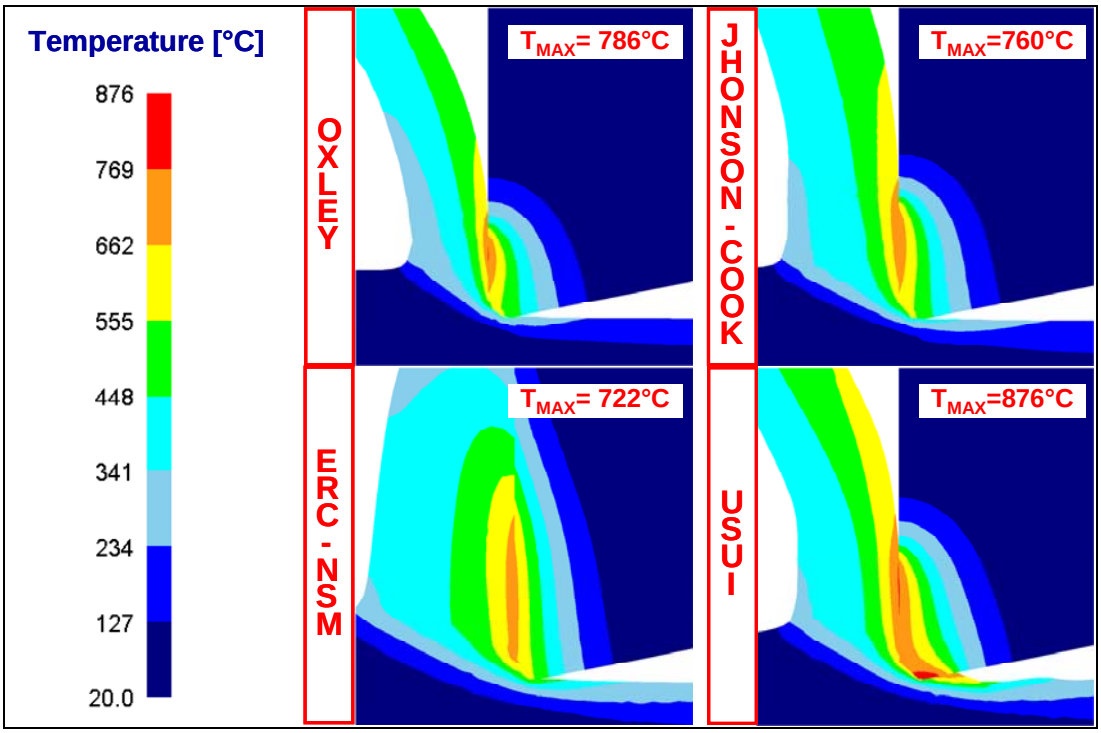

Figure 4.3. Predicted temperature in orthogonal cutting of AISI 1045 steel (V=150 m/min, f=0.1 mm/rev; Friction model: constant shear, m=0.82).

It is also well known in the cutting community that the simple ratio between cutting and thrust force is not accurately calculated.

At the same time, the thermal field is usually not well calculated, especially using Lagrangian formulation. This relevant inaccuracy may be due, also, to the material behaviour laws which are usually obtained by processes completely different respect to cutting. In fact, how it is well-known, to be useful in metal cutting simulation, flow stress data must be obtained at high strain rates (up to 10^6 s^{-1}), temperatures (up to 1000°C) and strain (up to 4). These data are impossible to reliably obtain with conventional tensile and compression tests. Often high speed Hopkinson's bar compression tests are used but these tests

require much effort and expensive equipment, and can provide data only for limited strain rates (up to 10^4 s^{-1}) and strain (up to 1.0 or less).

Taking into account all these considerations, a new strategy is proposed in this thesis, based on the use of some simple measures obtained during cutting process, i.e. cutting force, thrust force and temperature in the tool. The principal aim of this study is to locally model the material behaviour, in its real process conditions, and with very reduced costs. In this preliminary approach, for sake of simplicity, the problem was decomposed taking into account the reduced sensitivity of some variables on the material law. The latter was then obtained by an inverse approach using the results of a Lagrangian-Eulerian simulation and utilizing an optimization algorithm. The validity of the simplified material law was determined and its validity was verified in other cases. A satisfactory agreement between experimental and numerical data was found. The results will be presented in the following paragraphs.

4.2 METHODS TO DETERMINE FLOW STRESS AT HIGH STRAIN RATES

The material properties for metal cutting are obtained mainly using different methods, namely high-speed compression tests, Split Hopkinson's Pressure Bar (SHPB) tests, practical machining tests, integration of conventional tests at low strain rates and machining tests, and inverse analysis using FEA technique.

In high-speed compression tests [56,97], a compressed air pushes a punch to compress a specimen at a very high speed. The test specimen can be preheated in the furnace before the tests for obtaining material flow stress at elevated temperatures. However, maximum strain rate for this test is limited to about 450 s^{-1}. The heating rate in high-speed compression test is much slower than that in machining process and thus potentially causes anneal softening and/or age hardening of the sample. While, no such effects have been observed in practical machining [71].

Split Hopkinson's Pressure Bar (SHPB) technique was introduced in the early 20th century and has been further developed to study material behaviour (i.e. deformation, mechanical properties and fracture) at high deformation rates [98,99]. Later the SHPB test was adopted to determine the flow stress properties for machining processes [71,100]. Compared with high-speed compression tests, SHPB technique provides higher punch speed by the use of high-pressure air gun and faster heating rate by an induction coil. With these improvements, anneal softening and age hardening can be prevented, and the flow stress data at high strain rates up to 2,000 s^{-1} can be obtained [71]. Other applications of SHPB technique are performing high speed tension [101] and torsion tests [102] instead of compression tests. The strain and strain rate ranges in tension tests are typically lower than those obtainable in compression tests. Strains are up to 0.5 and strain rates are up to 500 s^{-1}. For torsion tests, the strain can be higher than 1, and strain rate can go up to more than 5000 s^{-1}. By modifying the sample geometry and testing in shearing mode, it is possible to achieve strain rates up to 10^4 s^{-1} [103,104].

However, strain-rate values obtained from SHPB tests are still lower than those reached in high speed machining (up to 10^6 s^{-1}). Moreover, SHPB tests can be costly and take considerable effort to obtain the data that are applicable in a wide range of strains and strain rates.

Several research groups have proposed to use machining tests to determine the flow stress data. Attempts were made to approximate the stress, strain, strain rate and temperature conditions that truly exist in machining. Analytical and/or empirical models were used to convert experimental data (i.e. cutting forces, thrust forces and chip geometry) into average stresses, strains, strain rates and temperatures of the plastic deformation zone in cutting, [105-107]. Shatla [108] introduced the inverse mapping method to indirectly determine the flow stress data by using Oxley's machining theory [56] and a minimization algorithm. Concept of his method is to minimize the error between the experimental forces (cutting and thrust forces) and the predicted forces from iterated flow stress parameters. Shatla's procedure requires relatively little experimental effort, but is

not able to generate a unique solution in all investigated cases. This method needs more computational robustness that can provide a unique solution.

In determining the flow stress data by machining tests, the reliability of the obtained flow stress data depends on the analytical models and assumptions employed to determine average stress and strain data in cutting. At the present, machining tests can provide only approximate flow stress data for hard metals that generate serrated chip formation since all available theoretical models still assume a continuous (non-serrated) chip.

Extrapolation of data from the tests conducted at various strain rate ranges have been suggested by some researchers [103,109-111]. The flow stress data obtained at low and high strain rates were fitted and represented by one or several flow stress equations. Thus, these obtained equations could be used to represent the flow stress for a wide range of strain rates. For example, tensile tests were conducted in a servo-hydraulic press to obtain the flow stress at the strain rates of 10-5 to 1 s-1, combined with the data from impact pendulum tests for the strain rates of 1 to 102 s-1 [111].

Inverse engineering method using FEA technique has been performed together with orthogonal turning tests to obtain the flow stress data [112,113]. Kumar [112] used the estimated flow stress data as input for FEM simulation of orthogonal cutting and modified the flow stress data until the predicted cutting forces agreed with experimental forces. The instantaneous flow stress data for each iteration was intuitionally selected by considering the difference between predicted force and experimental force. When the calculated and measured forces matched, the flow stress data is obtained. After Kumar, Özel [113] attempted to improve the flow stress determination method by changing both the flow stress data and the parameters used in the friction model until the predicted cutting force and thrust force were equal to those obtained from orthogonal turning experiments. This method, however, showed limit success due to non-unique solution of the problem and the fact that the flow stress solution is dependent on the FEM code.

Recently, Pujana et al. [114] presented a revision of different aspects concerning the inverse identification of flow stress employing cutting operations applied to the primary shear zone (PSZ). They also presented an approach for studying material's behaviour on the secondary shear zone (SSZ), employing two different steels (42CrMo4 and 20NiCrMo5) and finite element method simulations. The authors highlighted that the use of deterministic methods to optimize a set of constitutive parameters shows a dependency on the chosen starting point, because of the existence of relative optimums. Their study did not provide the desired results, supplying in the best case an overall error of 24% over the experimentally measured parameters.

4.3 THE PROPOSED PROCEDURE

The entire proposed procedure, detailed in the following paragraphs, is summarized in Figure 4.4.

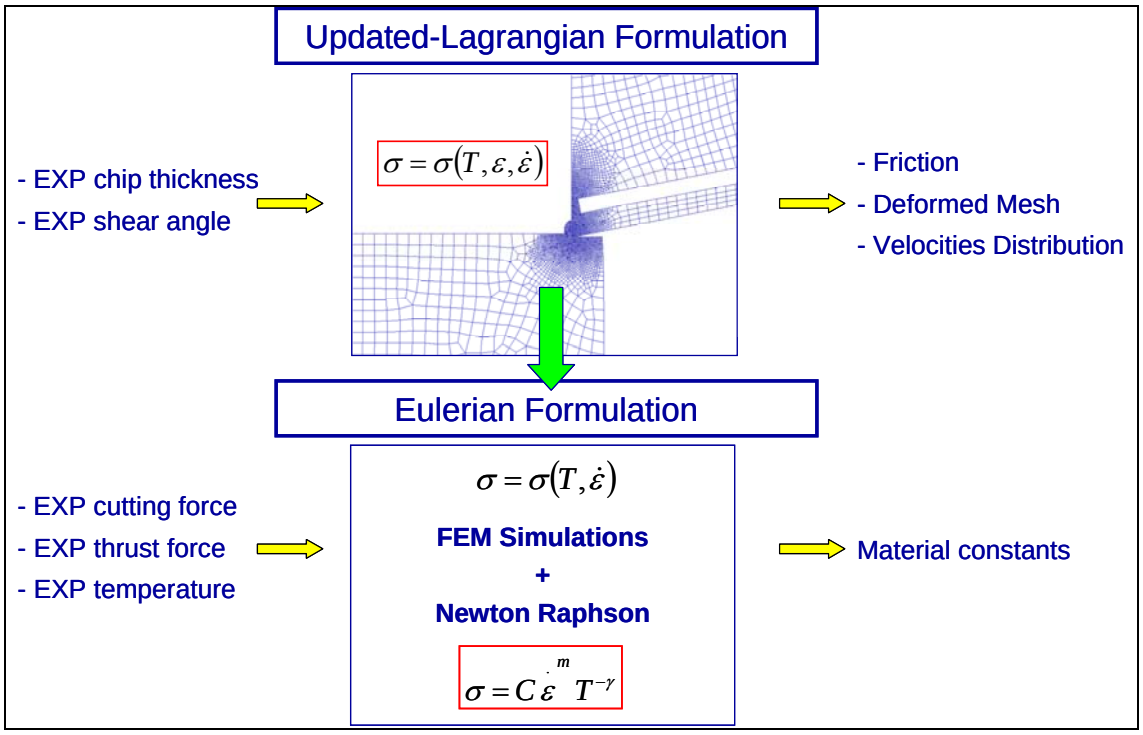

Figure 4.4. Inverse approach for obtaining the material law.

4.3.1 EXPERIMENTAL TESTS

As above introduced, an experimental investigation was preliminarily carried out in order to acquire reliable data to develop the procedure and to set-up the material model. In particular, cutting processes were run on a lathe, reproducing orthogonal cutting conditions (Figure 4.5).

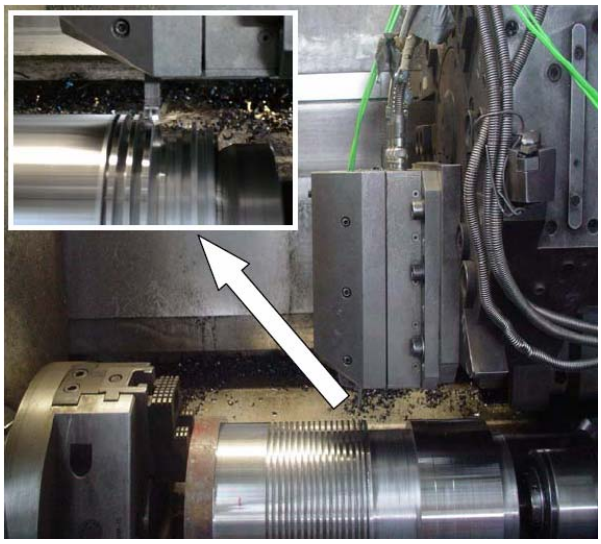

Figure 4.5. Experimental set-up.

The workpiece material was an AISI 1045 steel, while the cutting tool was an uncoated carbide ISO P30, with a rake angle of 0° and a relief angle of 6°. The tests were executed without any lubricant at the tool–chip interface, with the values of cutting speed and feed rate reported in Table 4.1.

Table 4.1. Cutting conditions.

Test case	1	2	3
Cutting speed V_c [m/min]	100	150	100
Feed f [mm/rev]	0.1	0.1	0.15

During the tests cutting and thrust forces were measured by using a piezoelectric dynamometer while an optical microscope was used to estimate the chip thickness. The temperature was measured using an embedded thermocouple, close to the cutting edge, at a distance of 0.6 mm from the rake face and 0.35 mm from the tool tip.

Table 4.2 shows the average experimental results in terms of cutting and thrust forces, chip contact length, chip thickness and shear angle.

Table 4.2. Experimental results.

Test case	1	2	3
Cutting force F_c [N]	745	715	1027
Thrust force F_t [N]	600	522	749
Chip thickness [mm]	0.288	0.220	0.355
Shear angle [deg]	19.0	24.4	23.0
Temperature [°C]	542	567	596

4.3.2 NUMERICAL PROCEDURE

In the present study the FEM commercial software "DEFORM-2D" was used to simulate orthogonal cutting. The reference cutting condition used was identified in test case 1 of Table 4.1 and Table 4.2.

Workpiece and tool sizes in simulation model were set large enough so that the predicted results were not sensitive to the boundary conditions. Figure 4.6 shows the FE model with the thermocouple socket position.

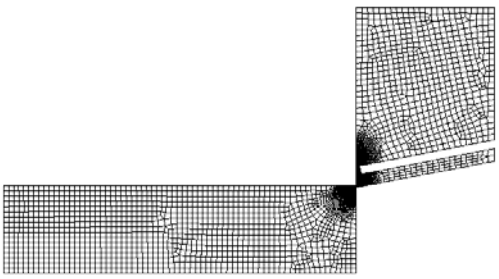

Figure 4.6. FE model.

An Updated-Lagrangian simulation was executed utilizing a well-known power law for the workpiece material. In particular, in this first case the employed model was the one proposed by Oxley [56], in which the effective flow stress is computed as an exponential function of the effective strain ε (Eq. 4.1):

$$\sigma = \sigma_1 \varepsilon^{n_1} \tag{1}$$

being σ_1 the strength coefficient and n_1 the strain-hardening exponent. Both σ_1 and n_1 vary with velocity-modified temperature T_{mod}, which couples the effects of strain rate $\dot{\varepsilon}$ and the temperature T_1. The concept of velocity-modified temperature was proposed by MacGregor and Fisher [68] and is defined as:

$$T_{\mathrm{mod}} = T_1 \left(1 - \nu \log \frac{\dot{\varepsilon}}{\dot{\varepsilon}_0} \right) \tag{2}$$

where ν and $\dot{\varepsilon}_0$ are constants that depend on the workpiece material and are readily available [1]. The relationship between T_{mod} and σ_1 and the relationship between T_{mod} and n_1 have been experimentally established for carbon steels using high speed compression tests [56].

The aim of this step was to find the friction model and the friction value in order to obtain a numerical shear angle as nearest as possible to the experimental one. In fact, an important assumption is here done, according with previous results: the chip-tool geometry is not relevantly dependent on the material law and thermal distribution. On the contrary, it's strongly related to friction coefficient. Thus, in this phase no thermal aspects were considered and the *h* value was set equal to zero. In particular the constant shear friction model with a coefficient equal to 0.98 permitted to obtain the minimum shear angle error.

Subsequently, an Eulerian analysis was run taking into account the Lagrangian step outputs. It's worth noticing, in fact, that both the deformed mesh and the velocity distributions were assumed as input for the Eulerian analysis. In this case the workpiece material behaviour was described by means of a simple law (Eq. 3) taking into account strain-rate and temperature:

$$\sigma = C \cdot \dot{\varepsilon}^{\,m} \cdot T^{-\gamma} \tag{3}$$

where C, m and γ are constants.

These constants were found utilizing an inverse procedure based on the optimization algorithm of Newton-Raphson. In particular, the three unknown

parameters were determined minimizing the objective function E, representing the difference between the experimental and corresponding computed cutting and thrust forces and temperature:

$$E = \sqrt{\left(\left(F_c^{\,num} - F_c^{\,\exp}\right)^2 + \left(F_t^{\,num} - F_t^{\,\exp}\right)^2 + \left(T^{\,num} - T^{\,\exp}\right)^2\right)} \tag{4}$$

where the numerical values derive from the Eulerian finite element simulation.

Of course, Eq. 3 introduces a strong simplification in the analysis, partially justified by the fact that a sensitivity analysis shown that the strain influence is lower than the others. In particular, in Eulerian frame all the data are not related with strain.

Finally, it was possible to identify the following material law:

$$\sigma = 970 \cdot \dot{\varepsilon}^{\,0.006} \cdot T^{-0.0225} \tag{5}$$

The application of this simple power law in Eulerian step of the turning process provided the results reported in Table 3 which also reports the prediction accuracy.

Subsequently, the law (Eq. 5) was used to predict the cutting and thrust forces such as the temperature in two new cases, with different cutting conditions. Also in these cases the procedure was the previously illustrated one. A Lagrangian simulation was performed, utilizing the Oxley's law to describe the AISI 1045 behaviour. The coefficient was determined in order to approach the experimental geometry. Also in these cases, the constant shear model and the friction coefficient equal to 0.98 allowed to minimize the errors. The relative errors for the shear angle were about 5% and 9% respectively. Table 4 reports the predicted variable at the end of the Eulerian simulation for a cutting speed of 150 m/min and feed equal to 0.1 mm/rev.

Forces, temperature and relative errors for a cutting speed of 100 m/min and a feed rate of 0.15 mm/rev are summarized in Table 5.

4.4 SOME CONSIDERATIONS

The preliminary proposed procedure provided satisfactory results, as it appears analyzing the data reported in the Tables 3-5. In fact, the average error is less than 10% and the researchers involved in this field surely agree to consider this discrepancy absolutely acceptable. Of course the calibration and validation procedures are not so robust at this state but the actual aim of this work is to propose a breaking procedure which starts from a different point of view respect to the traditional approaches.

Its main point of strength is the possibility to simulate the process in Eulerian environment, without knowing a priori the material flow rule. The latter can be directly derived by using simple steps if some mechanical and thermal data are available.

This way could constitute a point of discontinuity with the past since material is characterized in its real processing conditions thus it is intrinsically more robust and physically consistent. Temperature, strain and, mainly, strain rate are of the same order of the process ones, at difference of any other characterization test.

On the other hand, it is clear that substantial improvements will be necessary in terms of robustness and completeness.

4.4 CONCLUSIONS

The preliminary results of a study concerning material modelling through simple machining tests were presented. Nevertheless the strong simplification and the rough calibration and validation approach, the performance of the proposed procedure was verified comparing the numerical and experimental data.

In the future, the methodology has to be surely refined supplying a powerful procedure able to allow the simple calculation of the material constitutive low just measuring few experimental data.

CONCLUSIONS

Finite Element Method (FEM) based simulation is a very useful tool for obtaining relevant information in machining, difficult to acquire experimentally. Some examples are strain, strain rate, stress and temperature in both tool and machined workpiece. Anyway, the reliability of the results obtained from FEM simulation depends on the accuracy of the input values. For these reasons, numerical simulation of cutting process is still a very hard challenge since a lot of matters have to be taken into account. Although sometimes a strong geometrical simplification is done studying orthogonal cutting conditions (thus reducing the computational complexity), other aspects must be properly modelled in order to supply reliable result as simulation output. Among them, material behaviour, friction, energy conversion into heat and its propagation, definition of material damage criteria are just few examples that engage a number of scientists all over the World.

In this research work three main tasks contributing to the assessment of essential aspects of the numerical simulation of the cutting processes were conducted.

Accomplishments of this study can be summarized as follows:

- a wide analysis of the friction modelling was performed, at the varying of the workpiece/tool materials, material constitutive equations and cutting conditions. This study highlighted the significant role of friction in metal machining modelling, on the correct description of both mechanical and thermal phenomena. Machining has very severe friction conditions. Finite element modelling, to be useful, requires good friction

input data. At present a generally good predictive theory of friction is not available. This criticism is also related to the need of a better characterization of other crucial aspects: the thermal and the material modelling.

- a new approach to properly represent the thermal phenomena at the tool-chip interface was proposed. It included the definition of a physically-consistent model of the global heat transfer coefficient as function of process variables. This advanced approach was also adopted to obtain the numerical prediction of tool wear.
- an innovative procedure to characterize the material in its real process conditions was presented. It permitted to simulate the cutting process in the Eulerian environment, without any a priori knowledge of the material flow rule.

Concluding, it is important to underline that the results of this dissertation constitute an important contribution towards a better understanding and modeling of some fundamental aspects of cutting operations. But they also emphasize the necessity to improve the capability of machining simulations. This is a complex and challenging task for scientific research, but it also represents a key issue for the future development of such technologies.

REFERENCES

1. M. E. Merchant, 1998, *Mach. Sc. Tech.*, 2/2: 157-163.
2. P. Lorong, F. Micari, M. Touratier, 2007, Modelling of Cutting and Machining: 10 years of ESAFORM activity, Advances in Material Forming, Springer, 225-236.
3. E. J. A. Armarego, I. S. Jawahir, V. A. Ostafiev, P. K. Venuvinod, 1996, Modeling of Machining Operations, CIRP Working Group Paper, STC-C Paris, France.
4. C.A. van Luttervelt, T.H.C. Childs, I.S. Jawahir, F. Klocke, P.K. Venuvinod, 1998, Present Situation and Future Trends in Modelling of Machining Operations. Progress Report of the CIRP Working Group 'Modeling of Machining Operations', CIRP Annals, 47/2: 587-626.
5. W. Grzesik, Advanced Machining Processes of Metallic Materials. Theory, Modelling and Applications, 1st Ed., Elsevier, 2008.
6. W König, F. Klocke, M. Rehse, Prospects fort he use of process models in metal cutting, 1998, VDI Berichte, No. 1399, 235-249.
7. J. Mackerle, 2003, *Int. J. Mach. Tools & Manuf.*, 43: 103-114.
8. M.E. Merchant, Basic mechanics of the metal cutting process, 1944, J. Appl. Mech., 11: A168-A175.
9. M.E. Merchant, Mechanics of the metal cutting process, 1945, J. Appl. Phys., 16: 267-318.
10. V. Piispanen, Theory of formation of metal chips, 1948, J. Appl. Phys., 19: 875-881.
11. E.H. Lee, B.W. Shaffer, The theory of plasticity applied to a problem o machining, 1951, J. Appl. Mech., 18: 405-413.

12. H. Kudo, Some new slip line solutions for two-dimensional steady-state machining, 1965, Int. J. Mech. Sci., 7: 43-55.
13. W.B. Palmer, P.L.B. Oxley, Mechanics of orthogonal machining, 1959, Proc. Inst. Mech. Engrs., 173: 623-638.
14. P.L.B. Oxley, A.G. Humphrey, A. Larizadeh, The influence of rate of strain-hardening in machining, 1961, Proc. Inst. Mech. Engrs, 175:881-891.
15. E.D. Doyle, J.G. Horne, D. Tabor, Frictional interactions between chip and rake face in continuous chip formation, Proc. R. Soc. London A 366, 1979, 173-183.
16. K.J. Trigger, B.T. Chao, An analytical evaluation of metal cutting temperature, 1951, Trans. ASME 73: 57-68.
17. E. Usui, A. Hirota, M. Masuko, Analytical prediction of three dimensional cutting process. Part 1: Basic cutting model and energy approach, 1978, J. Eng. Ind., Trans. ASME, 100/2: 229-235.
18. S.M. Athavale, J.S. Strenkowski, Finite element modelling of machining: from proof-of-concept to engineering applications, 1998, Mach. Sci. Technol., 2/2: 317-342.
19. M.R. Movahledy, M.S. Gadala, Y. Altintans, Simulation of chip formation in orthogonal metal cutting process: an ALE finite element approach, 2000, Mach. Sci. Technol., 4/1: 15-42.
20. E.M. Trent, P.K. Wrigth, Metal Cutting, 4th Ed., B-Heinemann, 2000.
21. J.S. Strenkowski, J.T. Carroll, A finite element method of orthogonal metal cutting, 1985, Journal of Engineering Industry, Transaction of the ASME, 107: 346–354.
22. J.S. Strenkowski, G.L. Mitchum, An improved finite element model of orthogonal metal cutting, 1987, Proc North American Manufacturing Res Conf, Bethlehem, Pa, 506–509.
23. Z.C. Lin, S.Y. Lin, A coupled finite element model of thermal-elastic-plastic large deformation for orthogonal cutting, 1992, J Engng Ind., Trans. ASME, 114: 218–226.

24. Z.C. Lin, W.C. Pan, A thermoelastic-plastic large deformation model for orthogonal cutting with tool frank wear. Part I: Computational procedures, 1993, Int J Mech Sci, 35/10: 829–840.
25. Z.C. Lin, W.C. Pan, A thermoelastic-plastic large deformation model for orthogonal cutting with tool frank wear. Part II: Machining application, 1993, Int J Mech Sci, 35/10: 841–850.
26. Z.C. Lin, C.C. Liu, Analysis of orthogonal finish machining using tungsten carbide and diamond tools of different heat transfer coefficients, 1996, Int J Mach Tools Manufact, 36/1: 73–88.
27. Ueda, Manabe, Rigid-plastic FEM analysis of three-dimensional deformation field in chip formation process, 1993, Ann CIRP, 42/1: 35–38.
28. B. Zhang, A. Bagchi, Finite element simulation of chip formation and comparison with machining experiment, 1994, J Engng Ind, Trans. ASME, 116: 289–297.
29. J. Hashemi, A.A. Tseng, P.C. Chou, Finite element modeling of segmental chip formation in high-speed orthogonal cutting, 1994, J Mat Eng and Performance, 3/5: 712–721.
30. J.S. Strenkowski, J.T. III Carroll, An orthogonal metal cutting model based on an eulerian finite element method, 1986, Proc 13th NSF Conf on Prod Res and Tech, 261–264.
31. J.S. Strenkowski, K.J. Moon, Finite element prediction of chip geometry and tool/workpiece temperature distributions in orthogonal metal cutting, 1990, J Engng Ind, ASME, 112: 313–318.
32. K. Komvopoulos, S. Erpenbeck, Finite element modeling of orthogonal metal cutting, 1991, J. Engng. Ind., ASME, 113: 253–267.
33. T. Moriwaki, N. Sugimura, S. Luan, Combined stress, material flow and heat analysis of orthogonal micromachining of copper, 1993, Ann CIRP, 42: 75–78.

34. A.J. Shih, H.T. Yang, Experimental and finite element predictions of residual stresses due to orthogonal metal cutting, 1993, Int J Num Meth Eng, 36: 1487–1507.
35. A.J. Shih, Finite element simulation of orthogonal metal cutting, 1995, J Engng Ind, ASME, 117: 84–93.
36. A.J. Shih, Finite element analysis of orthogonal metal cutting mechanics, 1996, Int J Mach Tools Manufact, 36/2: 255–273.
37. V.S. Joshi, P.M. Dixit, V.K. Jain, Viscoplastic analysis of metal cutting by finite element method, 1994, Int J Mach Tools Manufact, 34/4: 553–571.
38. J.S. Wu, J. W. Dillon, W.Y. Lu, Thermo-viscoplastic modeling of machining process using a mixed finite element method, 1996, J Engng Ind, ASME, 118: 470–482.
39. K.W. Kim, H.C. Sin, Development of a thermo-viscoplastic cutting model using finite element method, 1996, Int J Mach Tools Manufact, 36/3: 379–397.
40. E. Ceretti, P. Fallböhmer, W.T. Wu, T. Altan, Application of 2D FEM to Chip Formation in Orthogonal Cutting, 1996, Journal of Materials Processing Technology, 59: 169-181.
41. I.S. Jawahir, Jr. O.W. Dillon, A.K. Balaji, M. Redetzky, N. Fang, Predictive Modeling of Machining Performance in Turning Operations, 1998, Proceedings of the 1st CIRP International Workshop on Modeling of Machining Operations, May 19, Atlanta, Georgia, USA, 161-176.
42. M. Shatla, Y.-C. Yen, T. Altan, Tool-workpiece Interface in Orthogonal Cutting – Application of FEM Modeling, 2000, Transactions of NAMRI/SME, XXVIII: 173-178.
43. R. M'Saoubi, H. Chandrasekaran, Innovative methods for the investigation of tool-chip adhesion and layer formation during machining, 2005, CIRP Annals, 54/1: 59-62.
44. P.T. Mativenga, N.A. Abukhshim, M.A. Sheikh, B.K.K. Hon, An investigation of tool-chip contact phenomena in high speed turning using

coated tools, 2006, Proc. IMechE, Part B: J. Engineering Manufacture, 220: 657-667.

45. N.A. Abukhshim, P.T. Mativenga, M.A. Sheikh, An investigation of the tool-chip contact length and wear in high speed turning of EN19 steel, 2004, Proc. Instn Mech. Engrs, Part B: J. Engineering Manufacture, 218: 889-903.
46. M.I. Sadik, B. Lindstrom, The role of tool-chip contact length in metal cutting, 1993, J. Mater. Processing Technol., 37: 613-627.
47. M.Y. Friedman, E. Lenz, Investigation of the tool-chip contact length in metal cutting, 1970, Int. J. Mach. Tools Des., 10: 401-416.
48. Y. C. Yen, Modeling of Metal Cutting and Ball Burnishing - Prediction of Tool Wear and Surface Properties, 2004, Ph. D. Dissertation, The Ohio State University, Columbus, Ohio.
49. H.-K. Tonshoff, C. Arendt, R. Ben Amor, Cutting of Hardened Steel, 2000, Annals of the CIRP, 49/2: 547-566.
50. Y.-C. Yen, A. Jain, T. Altan, A finite element analysis of orthogonal machining using different tool edge geometries, 2004, Journal of Materials Processing Technology, 146:72-81.
51. S. Kalpakjian, Manufacturing processes for engineering materials, 1997, Addison Wesley Publishing Company.
52. P. Sartkulvanich, F. Koppka, T. Altan, Determination of flow stress for metal cutting simulation—a progress report, 2004, Journal of Materials Processing Technology, 146: 61–71.
53. N.N. Zorev, Inter-Relationship between shear processes occurring along the tool face and shear plane in metal cutting, 1963, International Research in Production Engineering, ASME, 42-49.
54. E. Usui, T. Shirakashi, Mechanics of machining-from descriptive to predictive theory, 1997, *ASME Publ., PED Sciences,* 39: 369-389.
55. T.H. Childs, K. Maekawa, T. Obikawa, Y. Yamane, , Metal machining: theory and applications, 2000, Elsevier.

56. L.B. Oxley, Mechanics of Machining, an Analytical Approach to Assessing Machinability, 1989, Halsted Pr.
57. H. Bil, S.E. Kiliç, A.E. Tekkaya, A Comparison of Orthogonal Cutting Data from Experiments with Three Different Finite Element Models, 2004, International Journal of Machine Tools & Manufacture, 44: 933-944.
58. P. Sartkulvanich, T. Altan, A. Göcmen, Effects of Flow Stress and Friction Models in Finite Element Simulation of Orthogonal Cutting – A Sensitivity Analysis, 2005, Machine Science and Technology, 9: 1-26.
59. M. Shatla, C. Kerk, T. Altan, Process modelling in machining. Part II: validation and applications of the determined flow stress data, 2001, International Journal of Machined Tools & Manufacture, 41: 1659-1680.
60. T. Ozel, , The influence of friction models on finite element simulations of machining, 2006, International Journal of Machine Tools & Manufacture, 46: 518-530.
61. M.H. Dirikolu, T.H. Childs, K. Maekawa, Finite element simulation of chip flow in metal machining, 2001, International Journal of Mechanical Sciences, 43: 2699-2713.
62. Y.C. Yen, J. Söhner, B. Lilly, T. Altan, Estimation of Tool Wear in Orthogonal Cutting using the Finite Element Analysis, 2004, Journal of Materials Processing Technology, 146: 82-91.
63. L. Filice, D. Umbrello, F. Micari, L. Settineri, On the finite element simulation of thermal phenomena in machining processes, 2005, Proceedings of the 8th ESAFORM Conference, Cluj-Napoca, 729-732.
64. T.H.C. Childs, Material property needs in modeling metal machining, 1998, Machining Science and Technology, 2/2: 303-316.
65. T.H.C. Childs, R. Rahmad, , The need and a proposal for improved friction modelling in metal cutting, 2007, III International Conference on Tribology in Manufacturing Processes, Yokohama (Japan), 241-248.
66. Deform 2D User Manual, Scientific Forming Technologies Corporation Ed., Columbus (OH).

67. L. Filice, F. Micari, L. Settineri, D. Umbrello, On the finite element simulation of thermal phenomena in machining processes, 2007, *Adv. Methods Mater. Forming*, 263-278.
68. C.W. McGregor, J.C. Fisher, A Velocity-Modified Temperature for the Plastic Flow of Metals, 1946, ASME J. Appl. Mech., 13: 211-218.
69. G.R. Johnson, W.H. Cook, A Constitutive Model and Data for Metals Subjected to Large Strains, High Strain Rates and High Temperatures, 1983, VII International Symposium on Ballistics, The Hague (Netherlands).
70. S.P.F.C. Jaspers, J.H. Dautzenberg, Material behaviour in conditions similar to metal cutting: flow stress in the primary shear zone, 2002, Journal of Materials Processing Technology, 122/2-3: 322-330.
71. E. Usui, T. Shirakashi, K. Maekawa, Flow stress of low carbon steel at high temperature and strain rate (Parts I-II), 1983, Bulletin of the Japan Society of Precision Eng., 17: 161-172.
72. M.C. Shaw, Metal Cutting Principles, 2nd Ed., 2005, Oxford Science Publications.
73. N.N. Zorev, Metal Cutting Mechanics; 1966, Pergamon Press.
74. Y. Dogu, E. Aslan, N. Camuscu, A numerical model to determine temperature distribution in orthogonal metal cutting, 2006, J. Mat. Proc. Tech., 171: 1-9.
75. D. Umbrello, J. Hua, R. Shivpuri, Hardness Based Flow stress for Numerical Modeling of Hard Machining AISI 52100 Bearing Steel, 2004, Mat. Sc. Eng., A 374: 90-100.
76. E. Ceretti, L. Filice, F. Micari, Basic Aspects and Modeling of Friction in Cutting, 2001, Int. J. Forming Proc., 4/1-2: 73-87.
77. S. Lei, Y.C. Shin, F.P. Incropera, Thermo-mechanical modeling of orthogonal machining process by finite element analysis, 1999, Int. J. Mach. Tools Manuf., 39: 731–750.

78. J. Fleischer, J. Schmidt, L.J. Xie, C. Schmidt, F. Biesinger, 2D Tool Wear Estimation using Finite Element Method, 2004, Proc. of the 7th CIRP Int. Workshop on Modeling of Machining Operations, 82-91.
79. V.P. Astakhov, Metal Cutting Mechanics, 1999, CRC Press.
80. J. Yvonnet, D. Umbrello, F. Chinesta, F. Micari, A Simple Inverse Procedure to Determine Heat Flux on the Tool in Orthogonal Cutting, 2006, International Journal of Machine Tools & Manufacture, 46: 820–827.
81. Y.C. Yen, J. Söhner, J. Weule, J. Schmidt, T. Altan, Estimation of Tool Wear in Orthogonal Cutting using FEM Simulation, 2002, Mach. Sc. Tech. 6/3: 467-486.
82. P.R. Burte, Y.T. Im, T. Altan, S.L. Semiatin, Measurement and Analysis of Heat Transfer and Friction During Hot Forging, 1990, J. Eng. Ind., ASME, 332-346.
83. T.H.C. Childs, K. Maekawa , P. Maulik, Effects of Coolant on Temperature Distribution in Metal Machining, 1988, Materials Science and Technology 4/11: 1006-1019.
84. H.A. Kishawy, S. Kannan, M. Balazinski, Analytical modeling of tool wear progression during turning particulate reinforced metal matrix composites, 2005, Annals of CIRP, 54/1: 55-58.
85. S. Shimada, H. Tanaka, M. Higuchi, T. Yamaguchi, S. Honda, K. Obata, Thermo-chemical wear mechanism of diamond tool in machining of ferrous metals, 2004 Annals of CIRP, 53/1: 57-60.
86. H. Takeyama, T. Murata, Basic investigations on tool wear, 1963, J. Eng. Ind., Trans. of the ASME, 85: 33-38.
87. V.P. Astakhov, The assessment of cutting tool wear, 2004, Int. J. Mach. Tools Manuf, 44: 637-647.
88. C.Y.H. Lim, S.H. Lim, K.S. Lee, Wear of TiC-coated carbide tools in dry turning, 1999, Wear, 225-229: 354-367.

89. R. Ghosh, P.X. Li, X.D. Fang, I.S. Jawahir, An investigation of the effects of chip flow on tool-wear in machining with complex grooved tools, 1995, Wear, 184/2:145-154.
90. M. L. Penalva, M. Arizmendi, F. Díaz, J. Fernández, Effect of tool wear on roughness in hard turning, 2002, Annals of CIRP, 51/1:57-60.
91. E. Abele, A. Sahm, H. Schulz, Wear mechanism when machining compacted graphite iron, 2002, Annals of CIRP, 51/1:53-56.
92. L. Filice, D. Umbrello, F. Micari, L. Settineri, Wear modelling in mild steel orthogonal cutting when using uncoated carbide tools, 2007, Wear, 262/5-6:545-554.
93. K.-D. Bouzakis, I. Mirisidis, E. Lili, N. Michailidis, A. Sampris, G. Skordaris, Pavlidou, G. Erkens, I. Wirth, Impact resistance of PVD films and milling performance of coated tools at various temperature levels, 2006, Annals of CIRP, 55/1: 67-70.
94. P. Mathew, Use of predicted cutting temperatures in determining tool performance, 1989, Int. J. Mach. Tools Manuf., 29/4:481-497.
95. M.H. Attia, L.A. Kops, New approach to cutting temperature prediction considering the thermal constriction phenomenon in multi-layer coated tools, 2004, Annals of CIRP; 53/1:47-50.
96. T. Kitagawa, K. Maekawa, T. Shirakashi, E. Usui, Analytical prediction of flank wear of carbide tools in turning plain carbon steels. I: Characteristic equation of flank wear, 1988,Bulletin of the Japan Society of Precision Engineering, 22/4:263-269.
97. M. Oyane, F. Takashima, K. Osakada, H. Tanaka, The behaviour of some steels under dynamic compression, 1967, Proceedings of the 10th Japan Congress on Testing Materials, 72-76.
98. B. Hopkinson, The effects of momentary stresses in metals, 1905, Proceedings of Royal Society of London, A.74: 498-506.
99. H. Kolsky, An investigation of the mechanical properties of materials at very high rates of loading, 1949, Proceedings of the Physical Society, B 62: 676-700.

100. K. Maekawa, T. Kitagawa, T. Shirakashi, T.H.C. Childs, Finite Element Simulations of Three-Dimensional Continuous Chip Formation Processes, 1993, Proceeding of the 8th ASPE Annual Meeting, 519-522.
101. G.R. Johnson, W.H. Cook, Fracture Characteristics of Three Metals Subjected to Various Strains, Strain Rates, Temperatures and Pressures, 1985, Engineering Fracture Mechanics, 21/1: 31-48.
102. A. M. Eleiche, M.M. El-Kady, Modified Torsional Split Hopkinson Bar for the Cyclic Loading of Materials at Dynamic Strain Rates, 1983, in Novel Techniques in Metal Deformation Testing, Metallurgical Society of AIME, Warrendale.
103. C. Treppman, Fließverhalten Metallischer Werkstoffe bei Hochgeschwindigkeits beanspruchung, 2001, Dr.-Ing. Dissertation, RWTH Aachen, Germany.
104. E. El-Magd, C. Treppmann, Simulation of Chip Root Formation at High Cutting Rates by Means of Split-Hopkinson Bar Test, 1999, Materialpruefung (German Journal: Materials Testing), 41/11: 457-460.
105. P. Mathew, N.S. Arya, Material properties from machining, 1993, the 1st Conference on Dynamic Loading in Manufacturing and Service, Melbourne, Austraria, 33-39.
106. S. Lei, Y.C. Shin, F.P. Incropera, Material constitutive modeling under high strain rates and temperatures through orthogonal machining tests, 1999, Journal of Manufacturing Science and Engineering, 121: 577-585.
107. J. Kopac, M. Korosec, K. Kuzman, Determination of flow stress properties of machinable materials with help of simple compression and orthogonal machining test, 2001, International Journal of Machine Tools and Manufacture, 41/9: 1275-1282.
108. M. Shatla, C. Kerk, T. Altan, Process modeling in machining. Part I: Determination of flow stress data, 2001, International Journal of Machine Tools and Manufacture, 41/10: 1511-1534.

109. Y.B. Guo, C.R. Liu, Mechanical properties of hardened AISI 52100 steel in hard machining processes, 2002, Journal of Manufacturing Science and Engineering, 124/1: 1-9.
110. R. Stevenson, Study on the correlation of workpiece mechanical properties from compression and cutting tests, 1997, Journal of Machining Science and Technology, 1/1: 67-79.
111. L.W. Meyer, Strength and Ductility of a Titanium-Alloy TiAl6V4 in Tensile and Compressive Loading under Low, Medium and High Rates of Strain, 1984, Proceedings of the 5th International Conference On Titanium, Munich, Germany, 1851-1850.
112. S. Kumar, P. Fallböhmer, T. Altan, Computer Simulation of Orthogonal Metal Cutting Process: Determination of Material Properties and Effects of Tool Geometry on Chip Flow, 1997, Proceedings of NAMRC 1997, Lincoln, NE, SME Paper MR97-1.
113. T. Özel, T. Altan, Determination of workpiece flow stress and friction at the chip-tool contact for high-speed cutting, 2000, International Journal of Machine Tools and Manufacture, 40/1: 133-152.
114. J. Pujiana, P.J. Arrazola, R. M'Saoubi, H. Chandrasekaran, Analysis of the inverse identification of constitutive equations applied in orthogonal cutting process, 2007, International Journal of Machine Tools & Manufacture, 47:2153-2161.

ACKNOWLEDGEMENTS

First of all, I would like to express my sincere gratitude to my supervisor Prof. Luigino Filice, for the opportunity to work at the Manufacturing - TSL Group, for his continuous guidance throughout the course of this thesis work and for his patience.

A very special thanks also goes to Dr. Domenico Umbrello for his thrust, advices and hours of guidance and mentorship, both on this thesis project and in general. Without him, this thesis would not be what is today.

In addition, I thank Professor Fabrizio Micari, for his inestimable teaching during my PhD.

I thank Professor Francisco Chinesta for his hospitality and his teachings.

I extend my gratitude to Dr. Giusy Ambrogio, for her encouragement and friendship.

Thanks to Mr. Franco Pulice, Dr. Francesco Gagliardi and Mr. Leonardo Manco for their support and for making the working days fun.

And last but not least, I would like to acknowledge the encouragement, support, patience and love of my parents.